Doctor Thesis

Microscopic study of the charge fluctuation in α-(BEDT-TTF)$_2M$Hg(XCN)$_4$ probed by ^{13}C-NMR

(^{13}C-NMR 法による α-(BEDT-TTF)$_2M$Hg(XCN)$_4$ の電荷揺らぎの微視的な研究)

Ohnuma Akihiro

Low Temperature Physics Group,
Department of Condensed Matter Physics,
Graduate School of Science, Hokkaido University

2020 March

Contents

Chapter 1

Introduction

1.1 Organic conductor α-(BEDT-TTF)$_2X$

Organic conductors (BEDT-TTF)$_2X$ have quasi-two-dimensional electronic structure, where BEDT-TTF is bis(ethylenedithio) tetrathiafulvalene and X is a monovalent anion . BEDT-TTF molecules form conducting layers and anion X forms insulating layers, respectively. These are stacked alternately. BEDT-TTF molecules are interact to each other with overlapping of the π-orbits spreaded over the planar BEDT-TTF. The arrangement of the BEDT-TTF molecules dominates the electronic properties and the arrangement manner is represented by the Greek alphabet, κ, β, α, and so on (Fig.1.1). For example, κ-type salts showed the antiferromagnetic ordering or superconductivity, and α-type salts showed the charge ordering or density wave (CDW) state. Now we focus on an one of α-type salt modification.

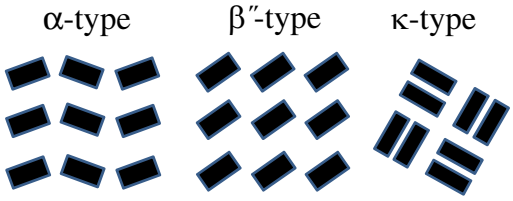

Figure 1.1: Arrangement of BEDT-TTF molecule in a conducting layer.

1.2 Crystal structure of α-(BEDT-TTF)$_2M$Hg(XCN)$_4$

Figure 1.2 shows the crystal structure of α-(BEDT-TTF)$_2M$Hg(XCN)$_4$ (M=Tl, K, Rb, and NH_4, X=S and Se), which is one of the α-(BEDT-TTF)$_2X$ series. Hereafter, the X=S series, α-(BEDT-TTF)$_2M$Hg(SCN)$_4$ (M=Tl, K, Rb, and NH_4) is abbreviated as α-Tl, α-K, α-Rb, and α-NH_4, re-

spectively. The X=Se series, α-(BEDT-TTF)$_2M$Hg(SeCN)$_4$ (M=Tl, K, Rb, and NH_4) is abbreviated as α-Tl(Se), α-K(Se), α-Rb(Se), and α-NH_4(Se), respectively. The salts of α-(BEDT-TTF)$_2M$Hg(XCN)$_4$ belong to the space group $P\bar{1}$ and have the three Crystallographically nonequivalent BEDT-TTF molecules, A, B, and C. A and A$'$ molecules are at general positions and connected by a inversion symmetry. B and C molecules, whereas, are located on a inversion center. In the conducting layer of α-(BEDT-TTF)$_2M$Hg(XCN)$_4$, there are two kinds of BEDT-TTF columns along c-axis and these columns alternate with each other along a-axis. One of them consists of A and A' molecules and the other consists of B and C molecules. The conducting layer is a-c plane.

The cell parameters of α-(BEDT-TTF)$_2M$Hg(XCN)$_4$ are listed in Table 1.1. These salts are isostructural with different anions. The cell volume can be explained with the ionic radius of the M and X ions in MHg(XCN)$_4$. The cell volume of the X=S series is smaller than that of the X=Se series reflecting the ionic radius of X. In the same X series, the cell volume with larger ionic radius of M is larger except in the case of α-Tl(Se) > α-K(Se).

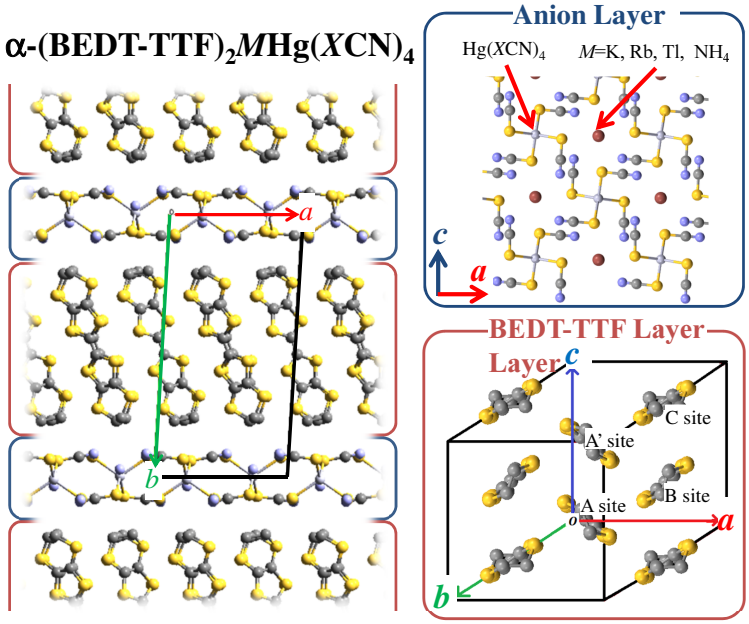

Figure 1.2: Crystal structure of the α-Rb.

	α-Tl	α-K	α-Rb	α-NH_4	α-K(Se)	α-Tl(Se)
space group	$P\bar{1}$	$P\bar{1}$	$P\bar{1}$	$P\bar{1}$	$P\bar{1}$	$P\bar{1}$
a(Å)	10.051(2)	10.082(10)	10.050(3)	10.091(1)	10.048(2)	10.105(1)
b(Å)	20.549(4)	20.565(4)	20.566(4)	20.595(2)	20.722(4)	20.793(1)
c(Å)	9.934(2)	9.933(2)	9.965(2)	9.963(1)	9.976(3)	10.043(1)
α(°)	103.63(1)	103.70(2)	103.57(2)	103.65(1)	103.59(2)	103.51(1)
β(°)	90.48(1)	90.91(4)	90.57(2)	90.53(1)	90.43(2)	90.53(1)
γ(°)	93.27(1)	93.06(4)	93.24(2)	93.30(1)	93.26(2)	93.27(1)
V(Å^3)	1990(1)	1997.0(21)	1998.5(8)	2008.1(3)	2015.2(9)	2047.9(8)
Ref.	[1]	[2]	[2]	[2]	[3]	[4]

Table 1.1: The cell Parameters of α-(BEDT-TTF)$_2M$Hg(XCN)$_4$.

1.3 Physical properties of α-(BEDT-TTF)$_2M$Hg(XCN)$_4$

1.3.1 Band structure

The band structures near the Fermi energy for α-(BEDT-TTF)$_2M$Hg(XCN)$_4$ are shown in Fig.1.3(a) [5]. The four upper bands are constructed from the four highest occupied molecular orbital (HOMO) of BEDT-TTF molecules, A, A', B, and C. There are two hole per unit cell with the formal charge of MHg(XCN)$_4^{-2}$. As a result, the system is regarded as a quarter filled system, and the two upper bands are partially filled and intersect with the Fermi level, suggesting that the higher band in the two upper bands constructs the 1-D FS, and the lower band constructs the 2-D FS as shown in Fig.1.3(b).

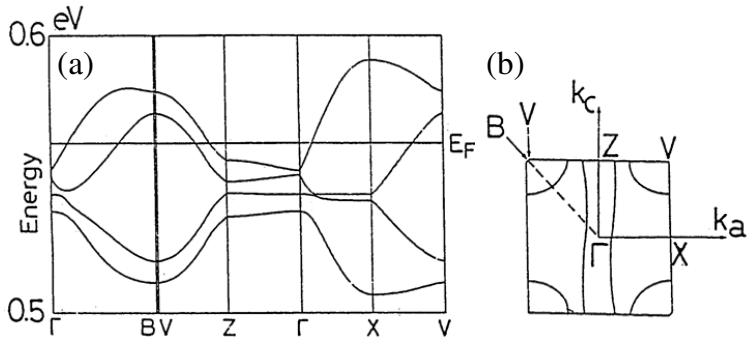

Figure 1.3: (a) The band structure and (b) FS of the α-Rb.

1.3.2 Resistivity

Figure 1.4(a), (b), (c), and Figure. 1.5 show the temperature dependence of the resistivity of the α-Tl, α-K, α-Rb, and α-NH_4 [6, 7, 8, 9]. In all X=S

salts, above about 10 K, the resistivity monotonically decreases with decreasing the temperature and metallic behavior is observed. In α-Tl, α-K, and α-Rb, a small hump is observed around 9 K, 8 K, and 12 K, respectively. This anomaly is also observed in other measurements. From the angle-dependent magnetoresistance oscillations (AMRO) measurement, the reconstruction of the FS was suggested below about 10 K [10, 11, 12]. The anomaly could be caused by the DW instability due to the nesting of the 1-D FS. There are two types of the DW states in quasi one-dimensional conductors, one of them is the spin density wave (SDW) and the other is the charge density wave (CDW). The SDW state is associated with the spin modulation, and the CDW state is associated with the lattice modulation. From the magnetic properties and X-ray diffraction (XRD) measurement, it was suggested that the DW state could be the CDW state.

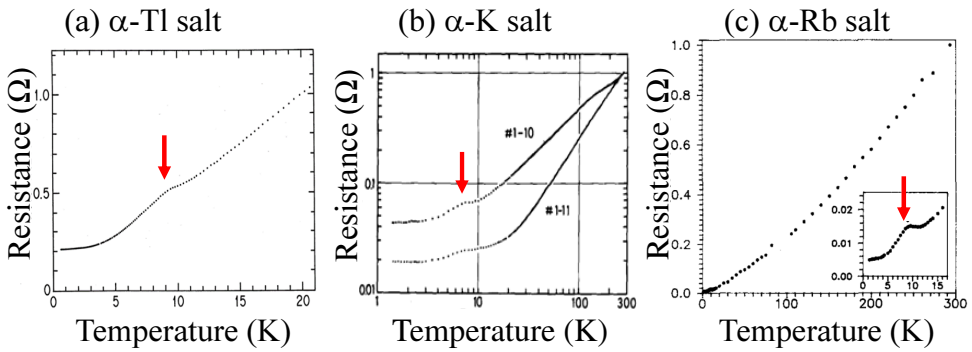

Figure 1.4: The temperature dependence of the resistivity in (a) α-Tl, (b) α-K, (c) α-Rb. The transition temperatures of the DW state are indicated with red arrows.

Whereas, in α-NH_4, no hump-like anomaly is observed and the SC transition is observed at around 1.4 K although the band structure in α-NH_4 is similar to those in α-Tl, α-K, and α-NH_4.

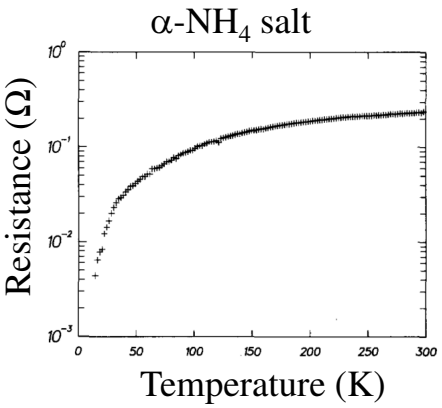

Figure 1.5: The temperature dependence of the resistivity in α-NH_4.

Figure. 1.6(a) and (b) show the temperature dependence of the resistivity of the α-Tl(Se) and α-K(Se), respectively [3, 13]. In the α-Tl(Se) and α-K(Se), no anomaly is observed around 10 K and the metallic behavior is observed in all temperature unlike the X=S series, suggesting that the α-Tl(Se) and α-K(Se) are a stable metal without any phase transition.

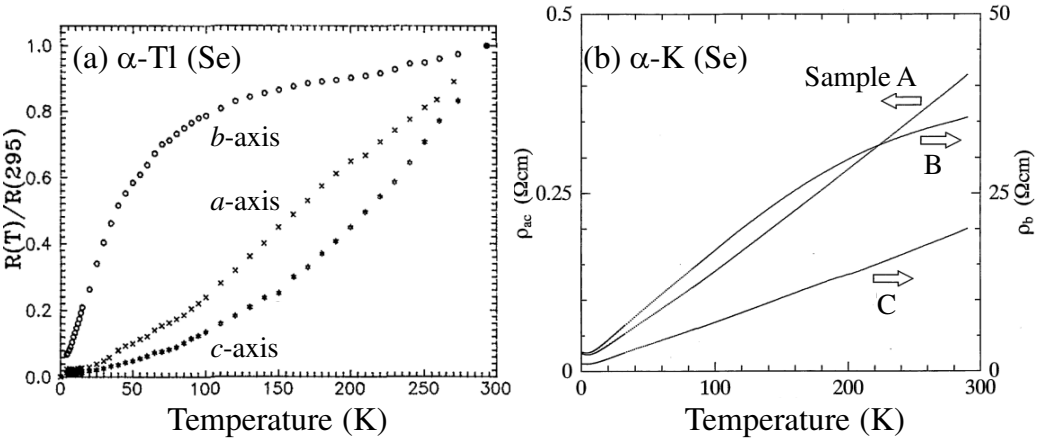

Figure 1.6: The temperature dependence of the resistance or resistivity in the (a) α-Tl(Se) and (b) α-K(Se).

1.3.3 Magnetic properties

Figure 1.7(a) shows the temperature dependence of the spin susceptibility of α-K, α-Rb, and α-NH_4 [14]. With decreasing the temperature, the spin susceptibility of the α-K and α-Rb monotonically decreases above 8

K (α-K) and 12 K (α-Rb), and drastically decreases at low temperatures, reflecting the decrease of the conduction carrier density due to the develop of the DW gap [15]. Whereas, the spin susceptibility of the α-NH_4 deviates from that of the α-K and α-Rb at around 150 K. Below about 150 K, the spin susceptibility of the α-NH_4 gradually increases and a small hump is observed at around 60 K, which could be connected to the freezing the rotation of the NH_4 molecule [16]. The steep decrease is not observed in the low temperature.

Figure 1.7(b) shows the temperature dependence of the $1/T_1T$ in X=S series, where T_1 is the spin-lattice relaxation time [14]. The $1/T_1T$ is roughly proportional to the spin susceptibility and the Korringa relation is completed. Hence, the electron correlation is not strong compared with the typical organic superconductor, κ-(BEDT-TTF)$_2$Cu(NCS)$_2$. At around the DW transition temperature of 10 K, no enhancement of the $1/T_1T$ is observed unlike the typical SDW transition. Hence the DW state in α-type salts seems not to be the SDW state.

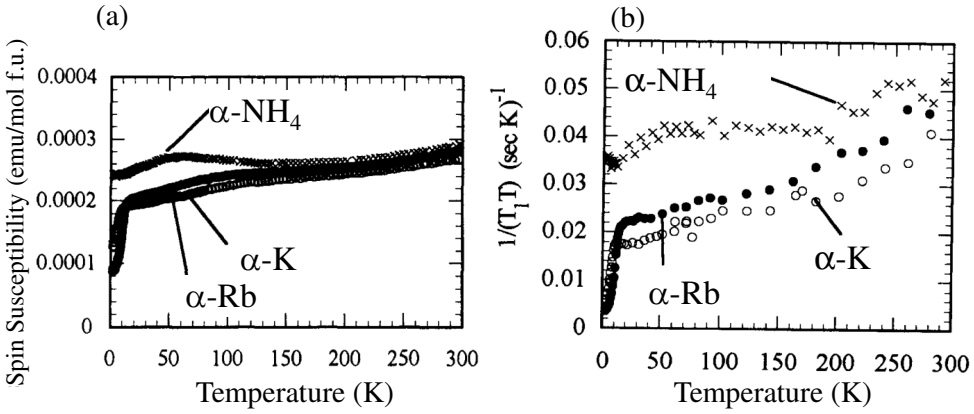

Figure 1.7: The temperature dependence of the (a) spin susceptibility and (b) $1/T_1T$ in α-type salts.

1.3.4 Uniaxial strain effect of α-(BEDT-TTF)$_2M$Hg(SCN)$_4$

In X=S series, an uniaxial strain parallel to the conducting $a-c$ plane control the ground state [17]. Figure 1.8(a) and (b) show the temperature dependence of the resistance of the α-K and α-NH_4 under the c-axial strain. The direction of the c-axial strain is shown in Fig. 1.8(c), and the $T_{\rm CDW}$ and $T_{\rm SC}$ is indicated as blue and red arrow in Fig. 1.8(a) and (b). In the α-K, the CDW anomaly around 10 K at ambient pressure is suppressed by applying c-axial strain, and the SC state is induced above the c-axial strain of 7 kbar. In the α-NH_4, the $T_{\rm CDW}$ of 1 K at ambient pressure increases up

to 6 K above the c-axial strain of 5 kbar. Hence the c-axial strain tends to induce superconductivity in the X=S series.

Figure 1.8(d) and (e) show the temperature dependence of the resistance of the α-K and α-NH_4 under the a-axial strain. The direction of the a-axial strain is shown in Fig. 1.8(f), and the T_{CDW} and T_{SC} is indicated as blue and red arrow in Fig. 1.8(d) and (e). In the α-K, the CDW anomaly is suppressed by applying a-axial strain similarly to the c-axial strain, and the metallic state is realized. In the α-NH_4, the SC state is suppressed by applying a-axial strain, and an hump-like anomaly is observed around 10 K under the a-axial strain of 4.5 kbar. The metallic state is realized above the a-axial strain of 6 kbar similarly to the α-K under the a-axial strain. From the AMRO measurement, the reconstruction of the FS is observed at low temperature under the a-axial strain of 4.5 kbar similarly to the α-Tl and α-K, suggesting the CDW transition. Hence the a-axial strain tends to induce the CDW and metallic state in the X=S series.

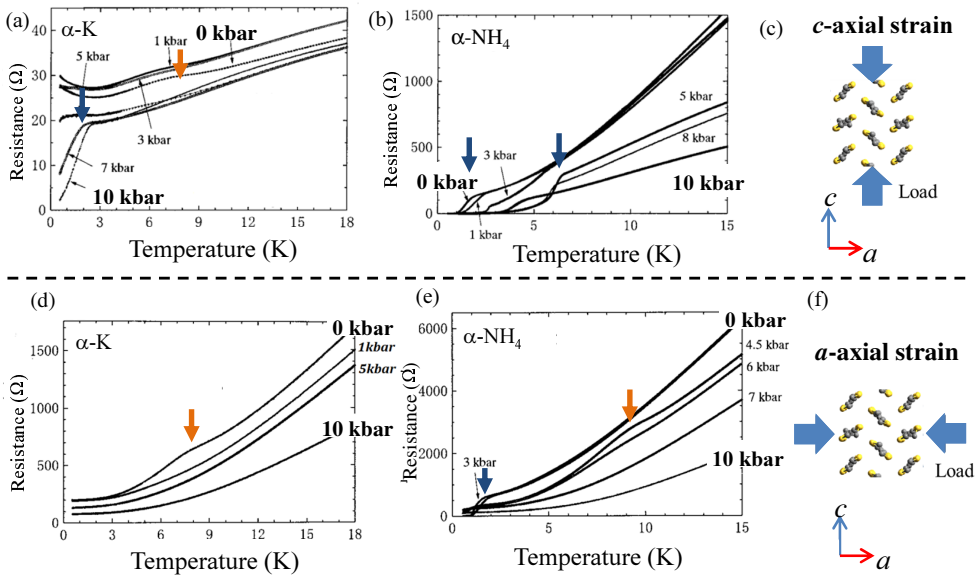

Figure 1.8: The temperature dependence of the resistance under the c-axial strain in the (a) α-K and (b) α-NH_4, and the temperature dependence of the resistance under the a-axial strain in the (d) α-K and (e) α-NH_4. The direction of the c-axial strain and a-axial strain are shown in Fig. 1.8(c) and Fig. 1.8(f), respectively.

These uniaxial strain effects are summarized in a phase diagram as shown in Fig. 1.9. The horizontal axis is the ratio of the lattice constant, c/a, and the vertical axis is the transition temperature of the SC, CDW, and metallic states. The c-axial strain decreases the lattice constant of the c-axis and

c/a, then the SC state is induced in the X=S series. Whereas the a-axial strain decreases the lattice constant of the a-axis and increase the c/a, then the CDW and metallic state are induced.

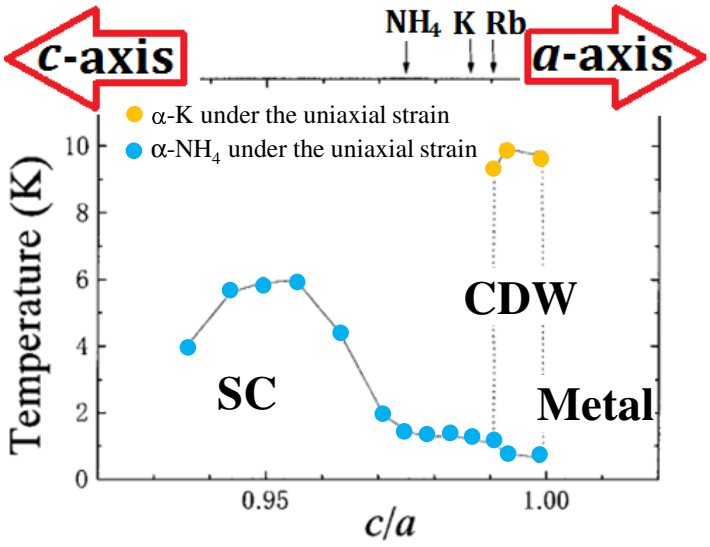

Figure 1.9: The Phase diagram of α-type salts. The horizontal axis is the ratio of the lattice constant, c/a, and the vertical axis is the transition temperature of the SC, CDW, and metallic states. Orange filled symbols are the results of the resistivity measurement in α-K under the uniaxial strain strain, and blue them are that in the α-NH_4 under the uniaxial strain.

1.3.5 XRD measurement

Figure 1.10(a) shows the X-ray photograph of the α-K at 10 K. The XRD measurement detected satellite reflections, $q_1 = (0.2(1), ?, 0.45(10))$, $q_2 = (0.4(1), ?, 0.1(1))$, and $q_3 = (0.5(1), ?, 0.5(1))$ [18]. The q_2 and q_3 is the second and third harmonics of a non sinusoidal incommensurate modulation q_1 within the error bar. The q_1 corresponds to the nesting vector calculated the band structure [10, 11].

Figure 1.10(b) and (c) shows the temperature dependence of the intensity of the q_3 and the temperature dependence of the correlation length of the q_3. The intensity of the q_3 shows the almost temperature independent behavior from 250 K to 10 K, and drastically increases below about the 10 K. The correlation length of the q_3 gradually increases with decreasing the temperature and saturates below about 50 K, then no anomaly is observed at around 10 K. The development of the lattice modulation is observed at around 10 K and should be caused by the CDW transition suggested from the AMRO measurement. However, in a conventional CDW state, the intensity and the

correlation of the satellite reflection drastically increase below the T_{CDW}. Whereas the correlation length in the α-Rb do not increase at around 10 K. Hence the CDW state in α-type salts seems to be unconventional.

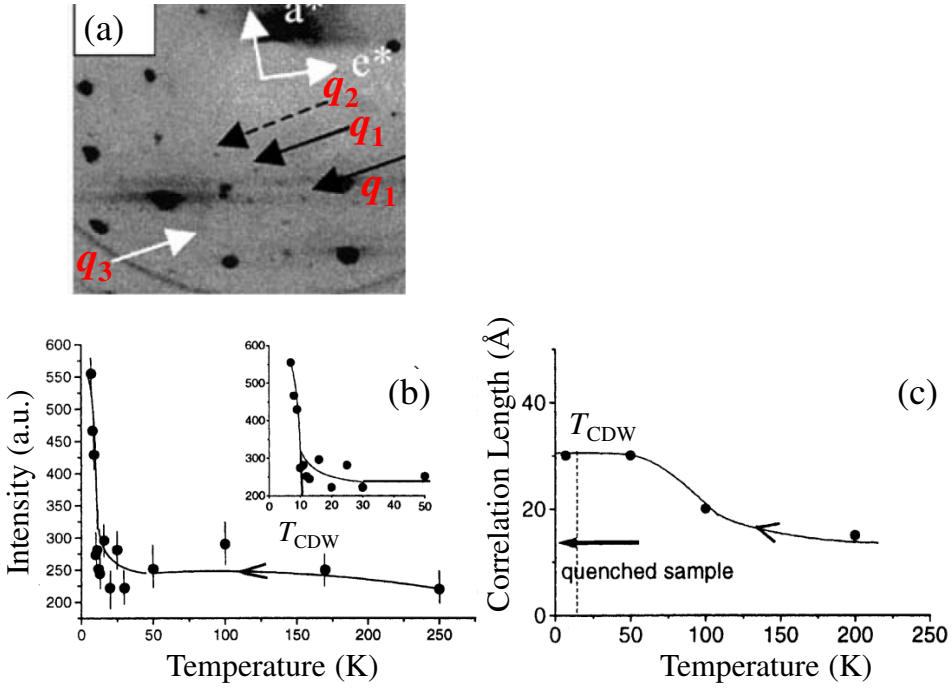

Figure 1.10: (a)The X-ray photograph of the α-K at 10 K. Satellite reflections, q_1, q_2, q_3 are observed. (b)The temperature dependence of the intensity of the q_3. (c)The temperature dependence of the correlation length of the q_3.

1.3.6 Optical studies

Additional anomalies were observed below $T^* = 200$ K. Figure 1.11(a) and (b) show the temperature dependence of the optical reflectivity and conductivity spectra of α-K, respectively. The optical conductivity was calculated by the Kramers-Kronig analysis. Below T^*, a significant dip around 200 cm^{-1} and pseudogap develops.

Figure 1.11(c) shows the theoretical calculation of optical conductivity. The peak around 2.0 of frequency could be due to the increase of the off-site Coulomb repulsion V and could correspond to the dip around 200 cm^{-1}, suggesting that the pseudogap may be due to the charge ordering (CO) or fluctuation caused by the V. The phase diagram where the superconductivity is mediated by the V was proposed [19, 20]. Theoretical studies also pointed

out that a charge frustration enhanced by the checkerboard charge pattern could induce the d_{xy}-wave paring superconductivity at quarter filling systems [21], suggesting there is the relationship between a charge pattern and paring mechanism of the superconductivity. It is important to reveal whether the pseudogap is due to the charge fluctuation or not and to reveal the charge pattern.

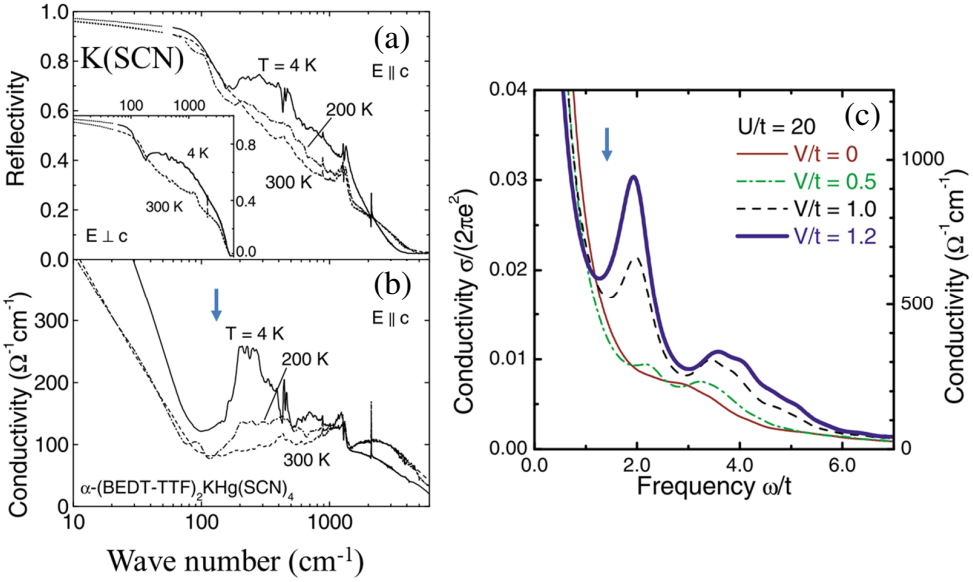

Figure 1.11: Temperature dependence of the optical (a) reflectivity and (b) conductivity spectra of α-K. (c)The theoretical calculation of the optical conductivity.

1.3.7 Previous NMR study on α-(BEDT-TTF)$_2M$Hg(SCN)$_4$

To reveal the charge disproportionation, site-selective ^{13}C-NMR measurements of α-Rb and α-NH_4 were performed [22, 23]. ^{13}C NMR measurement use the ^{13}C nuclei as the probe, and could reveal the microscopic electronic properties at each non-equivalent ^{13}C site. There are three non-equivalent BEDT-TTF molecules A, B, and C molecule in α-type salts as shown in Fig. 1.2. The A molecule locates on the general position. Whereas, the B and C molecule locate on the inversion center. Since the carbon sites of the central C=C bond on the A molecule are crystallography non-equivalent and those on the B and C molecule are equivalent, four NMR peaks from the each non-equivalent ^{13}C sites, A_a, A_b, B, and C, are expected to be observed.

Figure 1.12 shows the temperature dependence of the linewidth of NMR peak in the α-NH_4 (filled symbols) and α-Rb (open symbols). The linewidth of the B and C sites is almost temperature independent above $T^* = 200$

K, whereas the linewidth of the A site increase below T^*. The spin-spin relaxation time, T_2, was measured at each site and is almost temperature independent [22]. The linewidth of NMR peak is described as $\Delta\omega = 2\pi/T_2 + \gamma\Delta H$, here $\Delta\omega$ is the linewidth of NMR peak, T_2 is the spin-spin relaxation time, and ΔH is the inhomogeneity of the internal field. Hence the increase of the linewidth is caused by the development of the disproportionation between A molecules. This result suggested that the crystallographic symmetry would be broken between A molecules below $T^* = 200$ K. The inversion symmetry breaking at 200 K was also suggested by Raman spectroscopy [24], and supports the interpretation of the hump at around 200 cm^{-1} in the optical conductivity in the α-K [20].

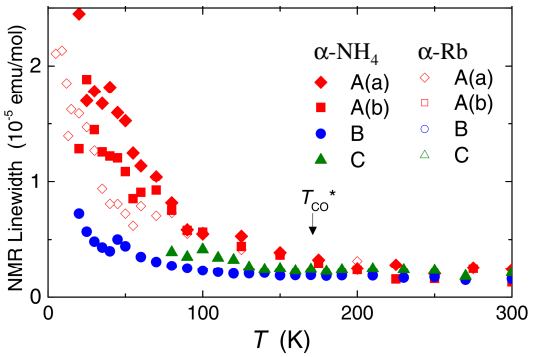

Figure 1.12: The temperature dependence of the linewidth of NMR peak at each site in the α-NH_4 (filled symbols) and α-Rb (open symbols).

1.4 Purpose

Below $T^* = 200$ K, the pseudogap was observed in α-K. The charge disproportionation and breaking of the inversion symmetry between A molecules are also observed. Because the inhomogeneity between B and C molecules also increased with decreasing temperature as shown in Fig. 1.13(a) [23], a phenomenon may be due to the development of horizontal stripe modulation below T^*, which means that B and C molecules become charge rich and poor sites, respectively, and A molecules also become charge rich and poor sites due to the inversion symmetry breaking (Fig. 1.13(b)). Actually, it was reported from x-ray diffraction(XRD) measurement that the horizontal stripe CO was realized in α-(BEDT-TTF)$_2$I$_3$ and θ-type salts [25, 26], which have same and similar BEDT-TTF molecular arrangement as α-(BEDT-TTF)$_2M$Hg(XCN)$_4$, respectively. However, because no anomaly due to the inhomogeneity between B and C molecules was observed below T^* in the CDW salt of α-Rb and SC salt of α-NH_4, it was unclear the charge pattern

and whether horizontal stripe modulation develops below T^*. To clarify the relationships among T^* anomalies, pseudogap and charge disproportionation, a general phase diagram and systematic NMR evaluation is needed of a reference salt that behaves as a simple metal on the phase diagram.

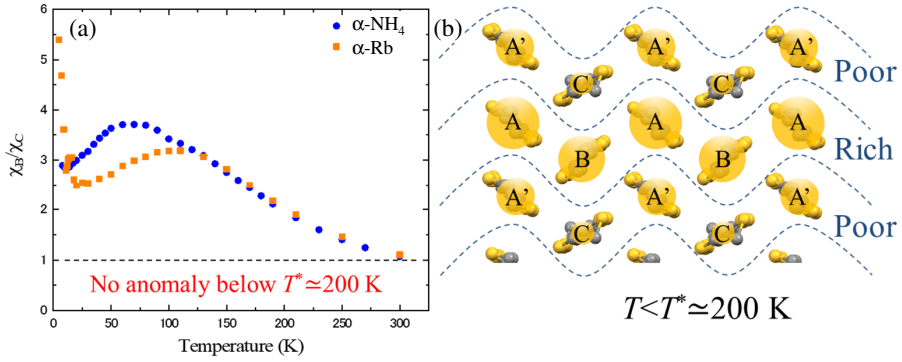

Figure 1.13: (a) Temperature dependence of χ_B/χ_C in α-NH_4 and α-Rb. (b) The schematic diagram of the horizontal stripe modulation below $T^* = 200$ K.

Generally, there are two methods to establish a general phase diagram. One method is the application of physical pressure and the other method is that of chemical pressure. In α-type salts, a uniaxial stran method, which is one of the physical pressure, realized the metallic state. However, the uniaxial strain method was unsuitable for NMR studies on the phase diagram. Figure. 1.14(a) and (b) show the temperature dependence of the NMR spectra of α-Rb salt under ambient pressure and under c-axial strain of 6 kbar, respectively. The linewidths broadened under the c-axial strain and we could not get separated NMR spectra because the pressure cell restricts the direction of the field.

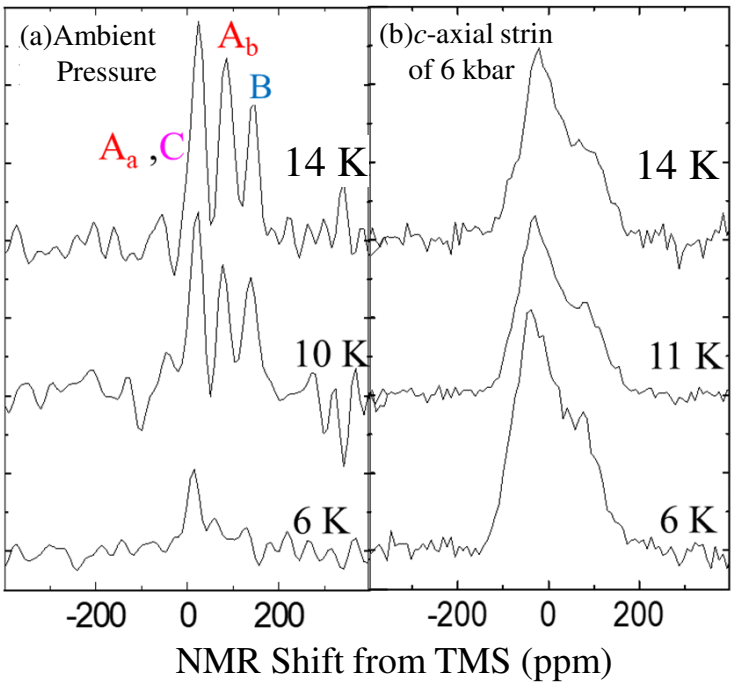

Figure 1.14: Temperature dependence of NMR spectra of α-Rb salt (a) under ambient pressure and (b) under c-axial strain of 6 kbar.

The chemical pressure method could be more suitable than the uniaxial stran method. The substituting the S atom by the Se atom realized the metallic state. The X=Se salts, however, show an only metallic state while the X=S salts show CDW and SC states but no salt shows a metallic state at low temperatures. We summarized the ground states of α-(BEDT-TTF)$_2M$Hg(XCN)$_4$ in Fig. 1.15. It was unclear the electronic state of the X=Se system can be described by the same phase diagram as that of the X=S system. The X=Se salt which shows a CDW or SC states had been required.

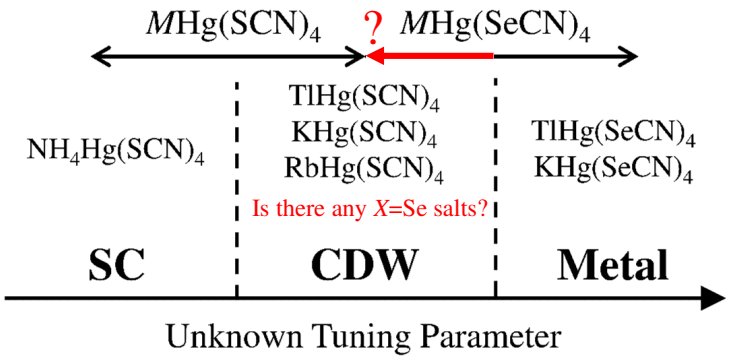

Figure 1.15: The summarized ground states of α-(BEDT-TTF)$_2M$Hg(XCN)$_4$. Because no X salt shows the CDW or SC states, the X=Se system was not linked to the X=S system.

In this thesis, firstly, we revealed that a new material α-NH$_4$(Se) shows CDW state at low temperature and could be a key material to link the X=S system to the X=Se system. Using the general phase diagram, we performed the NMR measurement in a metallic salt of α-Tl(Se). We revealed that the pseudogap of X=S salt could be due to the horizontal stripe modulation and the instability of the modulation may contribute the superconductivity.

Part I

Determination of the ground state of the α-(BEDT-TTF)$_2$NH$_4$Hg(SeCN)$_4$ and the general phase diagram

Chapter 2

Experiment

2.1 Synthesis

α-(BEDT-TTF)$_2$NH$_4$Hg(SeCN)$_4$ had not been synthesized because the anion of the NH$_4$SeCN is difficult to isolate and very sensitive to air and light in its solid state. The key to its preparation is the use of *liq*.NH$_3$ as a solvent. KSeCN (0.25 mol) was dissolved in *liq*.NH$_3$ (*ca*. 30 ml) at -70°, and was added to a solution of NH$_4$Cl (0.5 mol) in *liq*.NH$_3$ (ca. 30 ml) at -70° with argon purge. Then, small white KCl crystals were precipitated. When the mixture reached room temperature, the *liq*.NH$_3$ was removed. The resultant solids were extracted using a small amount of CH$_3$CN (*ca*. 30 ml). The CH$_3$CN solution was poured into dry ether (*ca*. 1 L). White precipitates (NH$_4$SeCN, 0.25 mol) were immediately collected and washed in ether. The NH$_4$SeCN salt was then dissolved in EtOH (*ca*. 100 ml) because of its sensitivity to air. This ethanol mixture of 2.5×10^{-3} mol/ml NH$_4$SeCN was used for the electrochemical oxidation. Single crystals of α-NH$_4$(Se) were prepared by electrochemical oxidation of BEDT-TTF, dissolved in 1,1,2-trichloroethane and 10 % volume absolute ethanol in the presence of a mixture of NH$_4$SeCN, Hg(SeCN)$_2$, and 18-crown-6. Electrical crystallization was conducted with Pt electrode (length : *ca* 10-20 mm, diameter : *ca* 1 mm) as shown in Fig. 2.1. The electrooxidation of BEDT-TTF was performed at a constant current of 8 μA at room temperature, and plate-like α-NH$_4$(Se) was obtained.

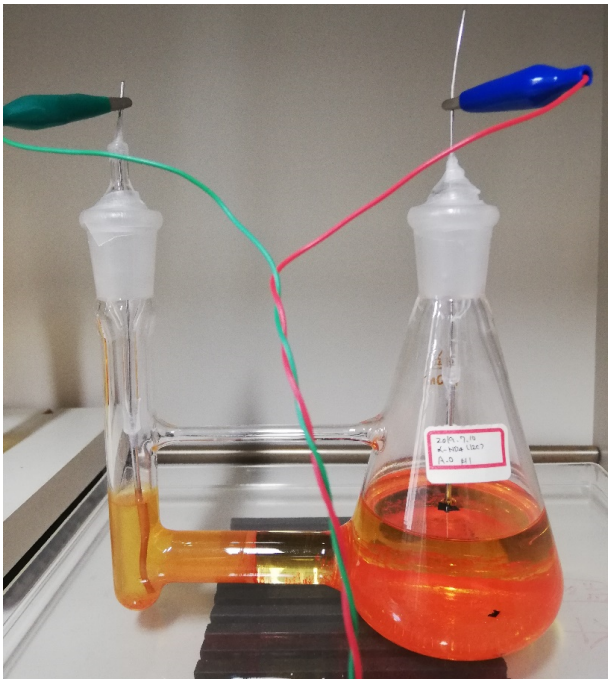

Figure 2.1: The cell of the electrochemical oxidation method with Pt electrode.

2.2 Crystal structure

To compare the crystal structure of α-NH_4(Se) with those of other α-type salts, we determined the crystal parameters not only of α-NH_4(Se) but α-Tl(Se), α-K, α-K(Se), α-NH_4, and α-Rb using the same XRD apparatus (Rigaku R-AXIS RAPID). XRD measurements were performed using graphite monochromated Mo-Ka radiation (λ=0.71075 Å). The crystal structures of α-NH_4 and α-NH_4(Se) were solved by the direct method (SIR2011) and refined on F^2 with full-matrix least-squares (SHELXL97) [27]. Because the NH_4^+ in the anion layer could rotate freely at room temperature, we could not determine the position of H^+ of the NH_4^+ in α-NH_4 and α-NH_4(Se).

2.3 Resistivity

Electronic resistance was measured in α-NH_4(Se) by the conventional four-probe DC method with the current parallel to the conducting layer from 300 K to 1.1 K.

2.4 Spin susceptibility

The static susceptibility of randomly-oriented crystals (20 mg) in α-Tl(Se), α-NH_4, α-NH_4(Se), and α-Rb was measured in a cooling and warming process with a commercially available SQUID magnetometer under an applied magnetic field of 10 kOe. We used two 1.5 mm square aluminum foils (15.4 mg) to wrap the crystals and used the straw to fix the position of the aluminum foils and crystals, which is a general method to perform a SQUID measurement. The static susceptibility of the crystals was evaluated by subtracting the paramagnetic contribution of background of the aluminum foils and straw and so on. Finally, the spin susceptibility was evaluated by subtracting the core-diamagnetic contribution from the static susceptibility according to Pascalś law.

Chapter 3

Results and Discussions

3.1 Crystal structure

The cell parameters of α-NH_4(Se) and c/a at room temperature are listed in Table 3.1 along with those of other α-type salts. All α-type salts were isostructural. In the previous studies in Table. 1.1 and Table. 3.1, the cell volume of the α-NH_4 was larger than that of the α-Rb nevertheless the ionic radius of the NH_4 is smaller than that of the Rb atom. Our systematic determination of the crystal parameters revealed that the cell volumes can be completely described by the ionic radius of the M and X atoms in MHg(XCN)$_4$.

Here we discuss the c/a of α-type salts at room temperature. The c/a at low temperatures could be related with the ground state intrinsically. On the other hand, the c/a at room temperature could also be related with the ground state; in fact, it was reported that the c/a of θ-type and κ-type salts at room temperature could tune ground state systematically [28]. While the c/a of the X=S salts line up from the SC salt to CDW salt, we could not find a systematic difference among the X=Se salts.

	a(Å)	b(Å)	c(Å)	α(°)	β(°)	γ(°)	V(Å^3)	c/a	Ref.
$TlHg(SCN)_4$	10.051(2)	20.549(4)	9.934(2)	103.63(1)	90.48(1)	93.27(1)	1990.0(1)	0.988(2)	[4]
$KHg(SCN)_4$	10.0279(4)	20.6095(9)	9.9318(4)	103.6104(13)	90.4660(13)	93.3304(13)	1991.11(15)	0.9904(4)	this work
$KHg(SCN)_4$	10.082(10)	20.565(4)	9.933(2)	103.70(2)	90.91(4)	93.06(4)	1997.0(21)	0.985(2)	[2]
$NH_4Hg(SCN)_4$	10.0934(5)	20.5877(10)	9.9675(5)	103.6366(15)	90.4884(18)	93.2897(15)	2009.03(18)	0.9875(5)	this work
$NH_4Hg(SCN)_4$	10.091(1)	20.595(2)	9.963(1)	103.65(1)	90.53(1)	93.30(1)	2008.1(3)	0.987(1)	[2]
$RbHg(SCN)_4$	10.0695(6)	20.5819(9)	10.0038(5)	103.6803(12)	90.4529(19)	93.2580(17)	2010.71(17)	0.9935(5)	this work
$RbHg(SCN)_4$	10.050(3)	20.566(4)	9.965(2)	103.57(2)	90.57(2)	93.24(2)	1998.5(8)	0.992(2)	[2]
$TlHg(SeCN)_4$	10.1071(5)	20.8080(8)	10.0547(4)	103.5337(9)	90.5059(12)	93.2675(12)	2052.00(14)	0.9948(4)	this work
$TlHg(SeCN)_4$	10.105(1)	20.793(3)	10.043(1)	103.51(1)	90.53(1)	93.27(1)	2047.9(8)	0.994(1)	[1]
$KHg(SeCN)_4$	10.0784(4)	20.8882(8)	10.0374(4)	103.5375(11)	90.5585(10)	93.3587(10)	2050.25(13)	0.9959(4)	this work
$KHg(SeCN)_4$	10.048(2)	20.722(4)	9.976(3)	103.59(2)	90.43(2)	93.26(2)	2015.2(9)	0.993(3)	[10]
$NH_4Hg(SeCN)_4$	10.1169(8)	20.8524(14)	10.0757(7)	103.5939(19)	90.584(2)	93.240(2)	2062.1(3)	0.9959(7)	this work

Table 3.1: Cell parameters of α-(BEDT-TTF)$_2M$Hg(XCN)$_4$.

The crystal structure of α-NH_4(Se) is depicted in Fig. 3.1. Conducting

BEDT-TTF and insulating anion layers are stacked alternately along the b-axis. In the conducting layer, there are three crystallographically nonequivalent BEDT-TTF molecules, A, B, and C in a unit cell as in the other α-type salts in Fig. 1.2. The S-S contacts shorter than the sum of the van der Waals radii in α-NH_4 and α-NH_4(Se) are shown in Fig. 3.2. The S-S contacts of α-NH_4(Se) are longer than that of α-NH_4 because substituting an Se atom for the S atom increases the unit cell volume.

Freezing of the rotation was reported by ^{2}D NMR [16]. The space around NH_4^+ affects the NH_4^+ rotation. The N-N distances between the NH_4^+ and XCN^- in α-(BEDT-TTF)$_2$$NH_4$Hg($X$CN)$_4$ are shown in Fig. 3.3. Different from S-S contacts, N-N distances in α-NH_4(Se) are shorter than in α-NH_4, suggesting the rotational barrier of α-NH_4(Se) is larger than that of α-NH_4.

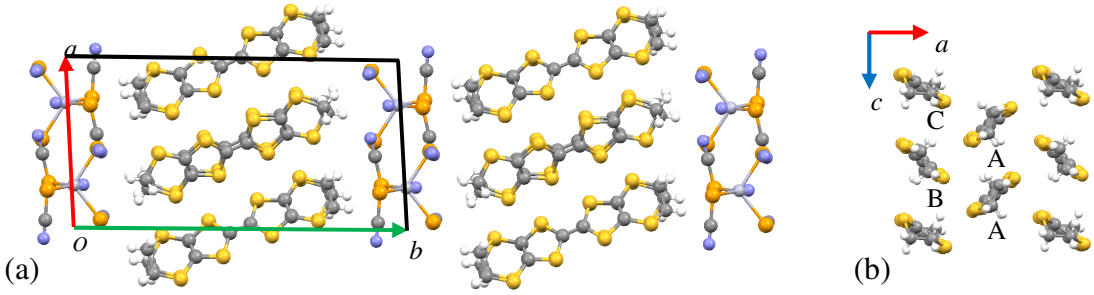

Figure 3.1: (a) Crystal Structure of α-NH_4(Se) viewed along the c axis. (b) Donor layer of α-NH_4(Se) viewed along the b axis.

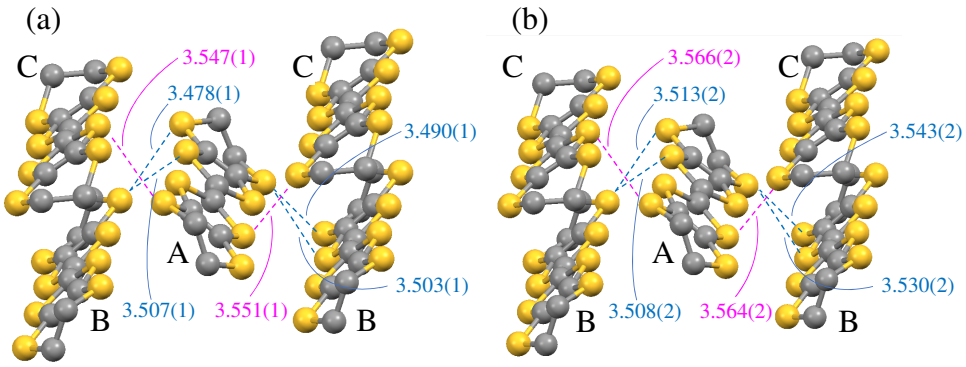

Figure 3.2: S-S contacts are shorter than the sum of the van der waals radii in (a) α-NH_4 and (b) α-NH_4(Se). S-S contacts between A and B molecules and those between A and C molecules are indicated as blue and pink broken lines, respectively.

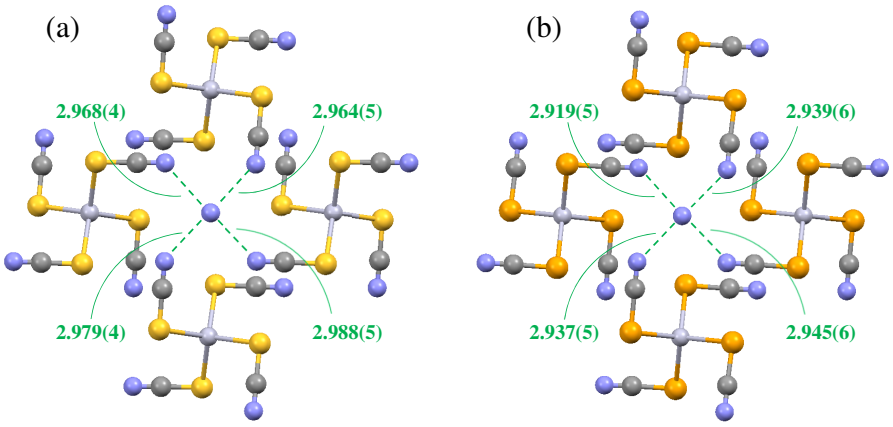

Figure 3.3: N-N distances between the NH_4^+ and $SeCN^-$ in the anion layer of (a) α-NH_4 and (b) α-NH_4(Se).

3.2 Band structure

The transfer integrals, band structure, and Fermi surface of the α-NH_4(Se) were calculated by extended Hückel-tight-binding approximation. The transfer integrals are listed in Fig. 3.4. The A and A' molecules are connected by inversion center symmetry. The transfer integrals of α-NH_4(Se) salt are almost the same as those of other α-type salts. However, the transfer integral c_1 of α-NH_4(Se) is about half that of α-NH_4. In the anion layer, the

$Hg(SCN)_4$ anions are located between A and A' molecules. Hence, it is considered that substituting an Se for an S atom increases the distance between A and A' molecules thereby decreasing c_1.

Figure 3.5 shows the band structure and the Fermi surface of α-$NH_4(Se)$. The Fermi surface of α-type salts consists of 1-D and 2-D Fermi surfaces as in other α-type salts (Fig. 1.3), hence one dimensional instability would be expected.

(a)

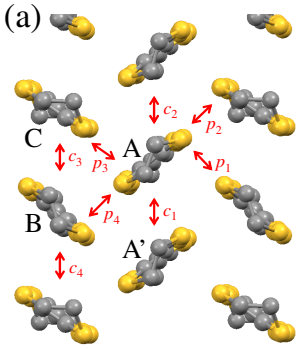

(b)

	$NH_4Hg(SeCN)_4$	$NH_4Hg(SCN)_4$
p_1 (eV)	0.091	0.086
p_2 (eV)	0.091	0.095
p_3 (eV)	-0.131	-0.137
p_4 (eV)	-0.126	-0.134
c_1 (eV)	0.014	0.024
c_2 (eV)	-0.060	-0.060
c_3 (eV)	0.009	0.009

Figure 3.4: Transfer integrals of α-$NH_4(Se)$.

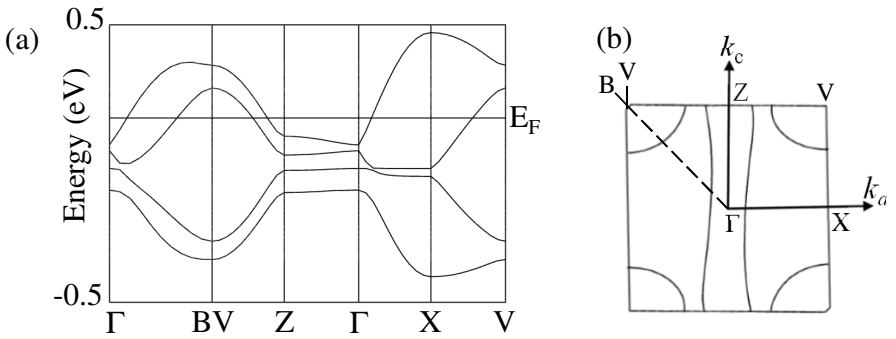

Figure 3.5: (a)The extended Hückel-tight-binding band structure and (b)the Fermi surface of α-$NH_4(Se)$.

3.3 Resistivity

Temperature dependence of the electric resistance of α-$NH_4(Se)$ is shown in Fig. 3.6. From electric resistance measurements, we can determine whether the CDW state is realized in X=S salts. α-Tl(Se) and α-K(Se) salts show

no phase transition or metallic behavior (Fig. 1.6) and α-NH_4 shows the SC transition below 1.5 K (Fig. 1.5). Whereas, α-Tl, α-K, and α-Rb are known to show metallic behavior with kink anomalies at low temperatures (Fig. 1.4), which are considered to be reconstructions of the Fermi surface due to the CDW transition.

The present α-NH_4(Se) salt shows metallic behavior above approximately 13 K and a kink change to semiconducting state.

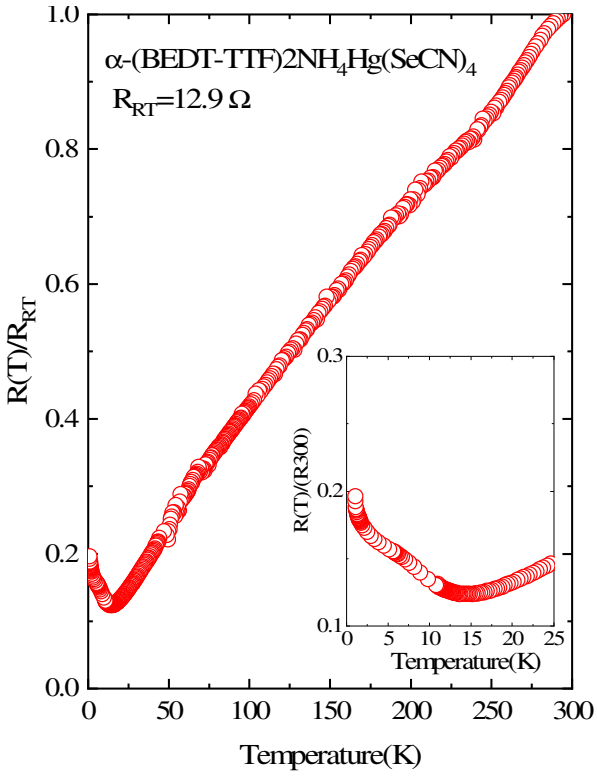

Figure 3.6: Temperature dependence of electric resistance in α-NH_4(Se).

3.4 Spin susceptibility

The characteristic feature of the CDW transition is a steep decrease in spin susceptibility below the transition temperature due to the formation of a spin singlet state (Sec. 1.3.3). The temperature dependence of the spin susceptibilities of α-NH_4(Se) along with those of other α-(BEDT-TTF)$_2M$Hg(XCN)$_4$ are shown in Fig. 3.7. Above around 150 K, all α-type salts display similar behavior and, except for α-NH_4, spin susceptibility decreases monotonically with decreasing temperature. The spin susceptibility

of α-Tl(Se) decreases monotonically showing no drastic change down to low temperatures. Similar to that of α-Tl, α-K, and α-Rb, the spin susceptibility of α-NH_4(Se) decreases drastically below around 12 K, suggesting that this anomaly of resistance is due to the CDW transition.

The spin susceptibility of α-NH_4 was shown to differ from those of other α-type salts around 150 K and showed a slight hump around 60 K accompanied by change in the molecular motion of NH_4^+ ions measured by ^{2}D NMR in α-NH_4 [16]. If the molecular motion of NH_4^+ ions affects the electronic state, similar behavior should be observed in α-NH_4(Se) at almost the same or a relatively higher temperature because the rotation barrier of α-NH_4(Se) is expected to be larger than that of α-NH_4. The spin susceptibility of α-NH_4(Se), however, does not show such deviation or feature below 150 K. This result suggests that the molecular motion of NH_4^+ ions could not significantly affect the electronic properties. To investigate the molecular motion of NH_4^+ ions in α-NH_4(Se), further studies such as ^{2}D NMR measurement in α-NH_4(Se) are desired.

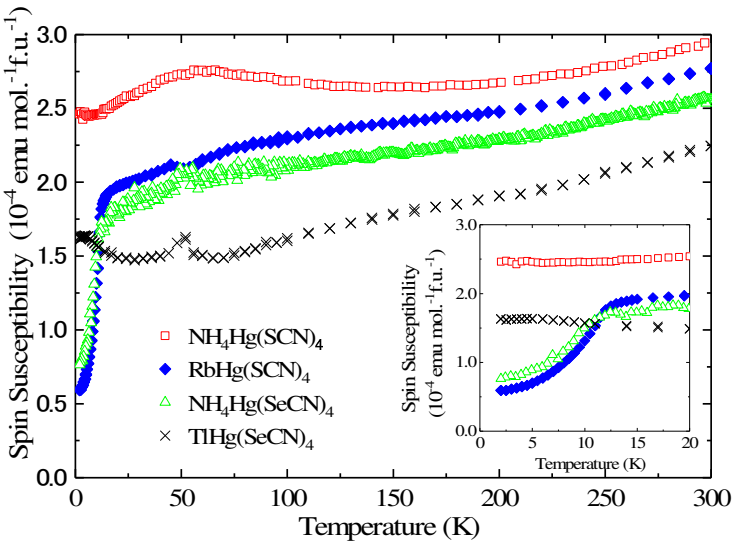

Figure 3.7: Temperature dependence of spin susceptibility of α-NH_4(Se) compared with those of α-(BEDT-TTF)$_2M$Hg(XCN)$_4$.

3.5 Ground state of the α-(BEDT-TTF)$_2$NH$_4$Hg(SeCN)$_4$

α-NH_4(Se) has 1-D and 2-D FS and is expected to have nesting instability as in other α-type salts. In α-NH_4(Se), the anomaly was revealed below about 13 K by resistivity measurement. Below this temperature, spin susceptibility decreased drastically, similar to the behavior of CDW salts. This

drastic decrease of spin susceptibility might have been caused by the spin-Peiels transition, SDW transition, or CDW transition. However, α-$NH_4(Se)$ showed metallic behavior down to just above the transition temperature, hence we can exclude the possibility of the spin-Peiels transition. Remaining possible causes of the ground state could be the SDW or CDW states. As for the SDW state, ^{13}C NMR spectra in α-$NH_4(Se)$ shown in Fig. 3.8 suggested the absence of an internal field at low temperatures as in other CDW salts [29]. These magnetic behaviors predict the ground state of α-$NH_4(Se)$ could be the same as the CDW state, and that α-$NH_4(Se)$ can connect the X=Se system to the X=S system.

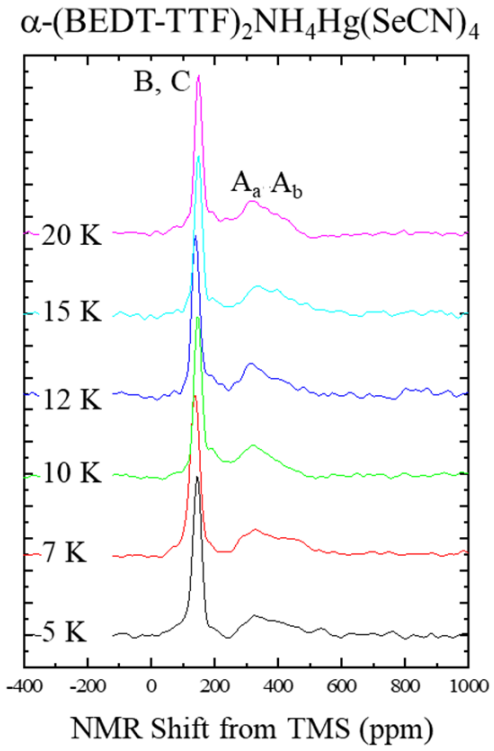

Figure 3.8: Temperature dependence of the NMR spectra at low temperature in α-$NH_4(Se)$.

Whereas the resistivity of the CDW salts shows a small hump around transition temperature and retains metallic behavior, that of α-$NH_4(Se)$ shows a smooth change to semi-conducting behavior below the transition temperature. Since resistivity may be sensitive to the nesting-condition of the 1-D FS, the slight difference in FS may have influenced resistivity at low temperatures. One of the anomalous characteristics in the CDW state is the short coherent length below the transition temperature from the satellite re-

flection in XRD measurement. The short coherence could enhance a disorder and affect the resistivity. The behavior of satellite reflection in α-NH_4(Se) is interesting.

3.6 Tuning Parameter of α-type salts

Since we confirmed the CDW state of α-NH_4(Se), the X=S and X=Se systems could be understood by the same phase diagram and connected with a universal phase diagram.

Note that the absolute values of spin susceptibility at room temperatures systematically change among SC salt of α-NH_4 and the metallic salt of α-Tl(Se). At room temperature, SC salt showed larger spin susceptibility than did metallic salt. The CDW salts of α-Rb and α-NH_4(Se) showed intermediate spin susceptibility. This systematic change in spin susceptibly suggested the metallic salt of α-Tl(Se) was not adjacent to SC but rather CDW salts.

Figure 3.9 shows a summary of our results. The X=S system covers the SC and CDW salts, whereas the X=Se system covers the CDW and metallic salts. The metallic salts of the X=Se system could not be adjacent to the SC salt but could be adjacent to CDW salts. The tuning parameter in α-type system however, remains unclear.

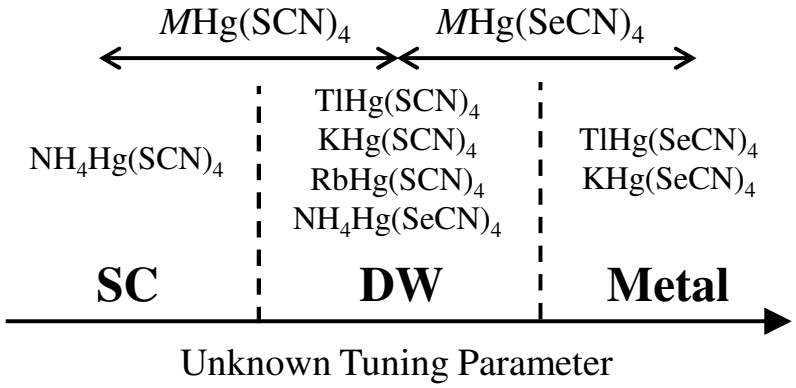

Figure 3.9: A schematic low temperature phase diagram of α-(BEDT-TTF)$_2M$Hg(XCN)$_4$.

We found no systematic difference in cell parameters among X=Se salts. We explored the tuning parameter for both X=S and X=Se salts from the crystal structures. To explore the tuning parameter, it is useful to compare α-type salts with θ-type salts [30]. The donor arrangements of α-type and θ-type salts are shown in Fig. 3.10(a) and Fig. 3.10(b), respectively. θ-type salts have a quarter-filled band as do α-type salts. In θ-type salts, it was

suggested that the dihedral angle (Θ) tunes the ground states because the transfer integral (p) decreases between adjacent stacks and bandwidth as the dihedral angle increases .

On the other hand, α-type salts have four kinds of transfer integrals between adjacent stacks, p_1, p_2, p_3, and p_4 as shown in Fig. 3.10(b) [5] whereas θ-type salts have only p. Both p_1 and p_4 are dominated by the dihedral angle between A and B molecules (Θ_B), and p_2 and p_3 by that between A and C molecules (Θ_C). Hence the bandwidth of α-type salts may be controlled by the two dihedral angles.

In θ-type salts, there is only one dihedral angle, which shows a negative correlation with c/a. Therefore, c/a is also a good tuning parameter for θ-type salts. However, in α-type salts, there are two dihedral angles, Θ_B and Θ_C, Θ_B shows a positive whereas Θ_C a negative correlation with c/a.

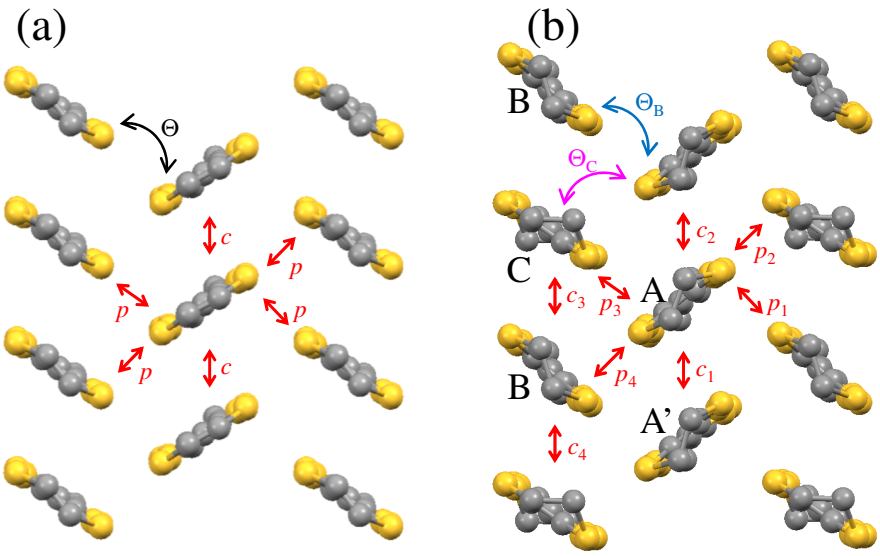

Figure 3.10: Donor arrangements of (a) θ-type and (b) α-type salts. Transfer integrals and dihedral angles are indicated by arrows.

We plotted the α-type salts on Θ_B-Θ_C coordinates as shown in Fig. 3.11. The SC, CDW, and metallic salts are indicated by circles, squares, and triangles, respectively. Most of the salts were plotted along a linear line. Since the A, B and C molecules cannot tilt independently because of steric repulsion among molecules, some relationship between Θ_B and Θ_C might be expected. The SC salt was located in the small Θ_B and large Θ_C regions, whereas the metallic salts were located in the large Θ_B and small Θ_C regions. The CDW salts were located in the intermediate Θ_B and Θ_C regions.

Here we discuss the relationship between the dihedral angle and electronic

state. In θ-type salts, it was suggested that a decrease in dihedral angle leads to an increase in transfer integral between adjacent stacks [30]. Based on the relationship between the dihedral angle and transfer integral, decrease in Θ_{B} and Θ_{C} could lead to an increase in transfer integrals between A and B (t_{B} =p_1 or p_4) and A and C molecules (t_{C} =p_2 or p_3), respectively. On the other hand, the off-site Coulomb repulsion between A and B molecules, $V_{\mathrm{A-B}}$, and that between A and C molecules, $V_{\mathrm{A-C}}$, would not change significantly because these would be dominated by the not angle between molecules but also distance. The dihedral angles may tune the degree of the charge disproportionation between A and B molecules, $V_{\mathrm{A-B}}/t_{\mathrm{B}}$ and that between a and C molecules, $V_{\mathrm{A-C}}/t_{\mathrm{C}}$. In this scenario, the SC salt is located in the large $V_{\mathrm{A-C}}/t_{\mathrm{C}}$ and small $V_{\mathrm{A-B}}/t_{\mathrm{B}}$ region. The previous NMR measurement revealed that the ratio of the DOS of A and that of B, $\chi_{\mathrm{B}}/\chi_{\mathrm{A}}$, in the SC salt is larger than that in the CDW salt [22, 23]. The large $\chi_{\mathrm{B}}/\chi_{\mathrm{A}}$ may be attributed to the small $V_{\mathrm{A-B}}/t_{\mathrm{B}}$. This scenario is one of the possibilities only from crystal structures.

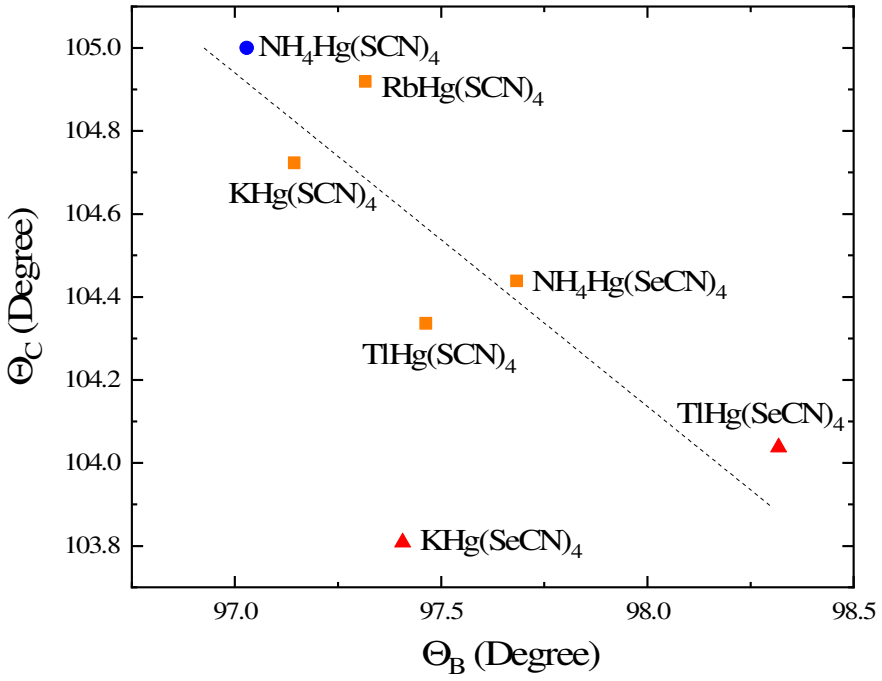

Figure 3.11: The Θ_{B}-Θ_{C} phase diagram of α-(BEDT-TTF)$_2M$Hg(XCN)$_4$. The horizontal and vertical axes are the dihedral angles between A and B molecules and A and C molecules, respectively. The blue circle, orange squares, and red triangles denote the SC, CDW, and metallic salts, respectively.

Chapter 4

Summary

We synthesized a new material of α-NH_4(Se) salt and revealed that α-NH_4(Se) showed the CDW state around 12 K as in α-(BEDT-TTF)$_2M$Hg(SCN)$_4$ salt (M=Tl, K, and Rb). This salt is the key material which links the X=S system to X=Se system and connects the X=S and X=Se systems to a universal phase diagram. We found Θ_B-Θ_C was a possible tuning parameter. The Θ_B and Θ_C of α-type salts could be plotted on a linear line. In this Θ_B-Θ_C plot, SC salt is located in the small Θ_B and higher Θ_C regions, whereas metallic salts are located in the small Θ_C and higher Θ_B regions. The dihedral angles may tune the degree of the charge disproportionation between A and B molecules, V_{A-B}/t_B and that between a and C molecules, V_{A-C}/t_C.

Spin susceptibility measurements indicated that the rotation of NH_4^+ could not affect the electronic state significantly.

α-NH_4(Se) enables us to perform the systematic NMR studies using metallic, CDW, and SC salt without restrictions inherent in the pressure cell. Following the results, we performed the ^{13}C-NMR measurement in the metallic salt of the α-(BEDT-TTF)$_2$TlHg(SeCN)$_4$ to reveal relationships among T^* anomalies, pseudogap and charge disproportionation.

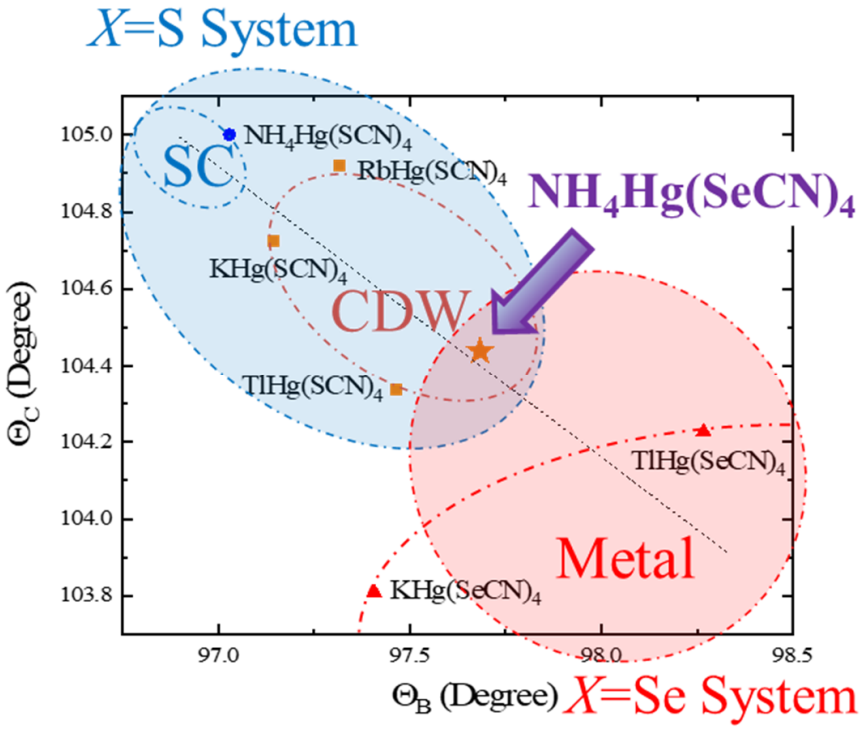

Figure 4.1: The Θ_B-Θ_C phase diagram of α-(BEDT-TTF)$_2M$Hg(XCN)$_4$. The X=S and Se systems are denoted by the blue and red regions, respectively. These systems are connected by the CDW salts of α-NH_4(Se).

Part II

^{13}C-NMR study of charge fluctuation in α-(BEDT-TTF)$_2$TlHg(SeCN)$_4$

Chapter 5

Experiment

A single crystal of the α-(BEDT-TTF)$_2$TlHg(SeCN)$_4$ was prepared with the electrochemical oxidation method as shown in Fig. 5.1. Because the crystal of the α-Tl(Se) tends to be twined along b^*-axis, we carefully chose a single crystal. In this molecule, one side of the central C = C bond was selectively enriched with ^{13}C to prevent the NMR peak splitting due to the Pake doublet [Fig. 6.1(a)] [31]. NMR spectra were obtained using a spin-echo method with an external magnetic field of 6.1 T. The angular dependence of the NMR shift was measured with rotation around b^* axis (θ = 0^o: a-axis, θ = 90^o: $c' = a \times b^*$-axis). Because the hyperfine coupling constants of A and B, C molecules are large at θ = 54^o and θ = 127^o [22], the line widths and NMR shifts of A, B, and C sites were measured at θ = 54^o and θ = 127^o, respectively. Atomic parameters of α-type salts, α-Rb, α-NH$_4$, and α-Tl(Se), needed to estimate local spin susceptibilities from NMR shifts were assessed with XRD measurements (Rigaku R-AXIS RAPID) with Mo K-α radiation of λ = 0.71075 Å.

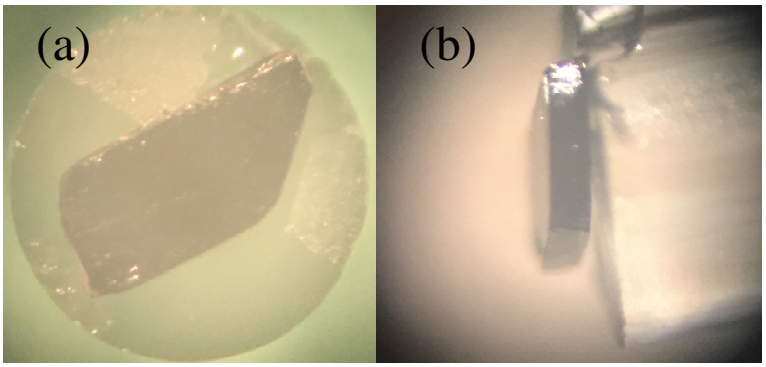

Figure 5.1: A single crystal of the α-Tl(Se) viewed along the (a) b^*-axis and (b) a-c' plane.

Chapter 6

Results and discussions

6.1 Site assignment and determination of hyperfine coupling constant

The α-type salts contain three nonequivalent BEDT-TTF molecules, A, B, and C (Fig. 6.1(b)), with the A molecule located in a general position and B and C molecules located in the inversion center. Because the carbon atoms of the central C = C bond on the A molecule are crystallographically nonequivalent, whereas those on the B and C molecules are equivalent, the nonequivalent ^{13}C sites, A_a, A_b, B, and C, appeared as four NMR peaks (Fig. 6.2, inset). As the NMR shift is maximal when the external field is parallel to the p_z orbital, these NMR peaks could be assigned by the angular dependence of the NMR shifts. Figure 6.2 shows the angular dependence of the NMR shift of α-Tl(Se) around the b^*-axis at 250 K. The horizontal axis is the angle of the external field from the a-axis ($\theta = 0^o$) to the c'-axis ($\theta = 90^o$). The curves for the closed black circles, the red squares, the blue triangles, and the pink inverted triangles were assigned to the A_a, A_b, B, and C sites, respectively.

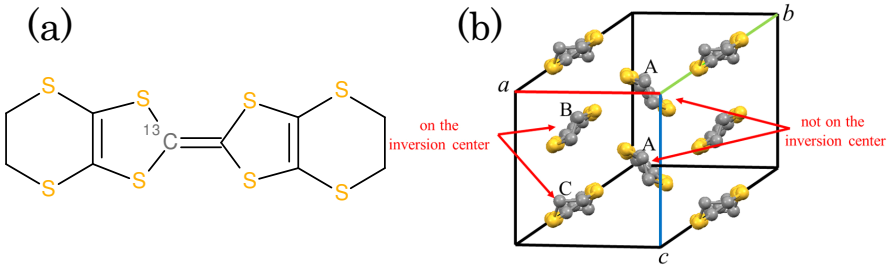

Figure 6.1: (a)Molecular structure of BEDT-TTF. The molecule was selectively enriched in ^{13}C to prevent the Pake doublet effect. (b) Donor layer of α-type salts viewed along the b-axis.

The NMR shift can be expressed using the equation $\delta(\theta) = K_{\rm spin}(\theta)+K_{\rm vv}(\theta)+\sigma(\theta)$, where θ is the field direction from the a-axis to the c'-axis, $K_{\rm spin}(\theta)$ is a spin term of the Knight shift, $K_{\rm vv}(\theta)$ is a Van Vleck term of the Knight shift, and $\sigma(\theta)$ is a chemical shift. As for BEDT-TTF compounds, the Van Vleck term is negligible because the splitting in the energy levels between the $2p_{\rm z}$ orbital of the central C=C bond (π) and unoccupied $2p_{\rm x}$, $2p_{\rm y}$ orbitals (σ^*) is large and the secondary perturbation is significant small unlike the cuprate compounds, which have almost degenerate states due to the small crystal field [32]. Hence, we can neglect the Van Vleck term and the NMR shift is described as $\delta(\theta) \simeq K_{\rm spin}(\theta)+\sigma(\theta) = A(\theta)\chi_{\rm s} +\sigma(\theta)$, where $\chi_{\rm s}$ is a local spin susceptibility and $A(\theta)$ is a hyperfine coupling constant.

The chemical shift could be estimated from the chemical shift tensor for $(\text{BEDT-TTF})^{+0.5}$ molecule [33]. The angular dependence of the Knight shift for each site could be calculated by subtracting the chemical shift from the observed NMR shift. The temperature dependence of the local spin susceptibilities, $\chi_{\rm s}$, could be determined by measuring a Knight shift large enough to be observed. The angles θ most suitable for the A and the B and C sites were found to be 54° and 127°, respectively (Fig. 6.2, dashed line). Therefore, to evaluate local spin susceptibilities, it was necessary to determine the hyperfine coupling constants at the corresponding angles.

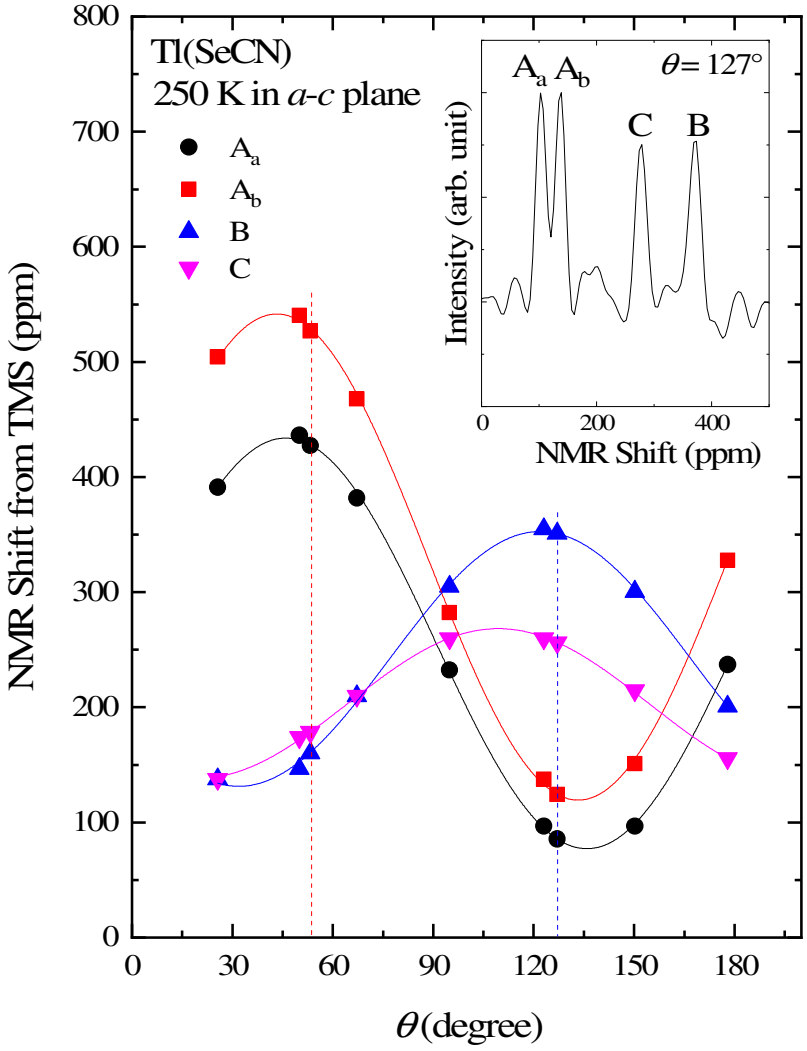

Figure 6.2: Angular dependence of the NMR shift of the α-Tl(Se) around the b^*-axis at 250 K. The dashed lines denote the field direction of the θ =54° and 127°. The inset shows the NMR peaks of each nonequivalent ^{13}C sites, A_a, A_b, B, and C at θ =127°.

Hyperfine coupling constants were determined with the following analysis. The anisotropy of the Knight shift mainly depends on the anisotropy of the hyperfine coupling constant, which is primarily due to the p_z orbital of the BEDT-TTF molecule. Thus, the amplitude of the Knight shift is likely proportional to the local spin susceptibility. The ratios of local spin susceptibility determined from the angular dependence of the Knight shift [34], could be expressed as χ_A (250 K) : χ_B (250 K) : χ_C (250 K) = 1 : 0.66

: 0.46, with the amplitude at the A site being the mean of the amplitudes of the A_a and A_b peaks, and with the amplitudes of the B and C peaks. From total spin susceptibilities measured using a SQUID magnetometer ($\chi_{SQUID} = \frac{1}{2}\chi_{All} = \frac{1}{2}(2\chi_A + \chi_B + \chi_C)$) [35], we estimated the local spin susceptibilities to be χ_A (250 K) = 6.7 × 10^{-5} emu/mol, χ_B (250 K) = 4.4 × 10^{-5} emu/mol, and χ_C (250 K) = 3.1 × 10^{-5} emu/mol. Using the chemical shift of 59.8 ppm for the A site at 54° and those of 60.2 ppm for the B site and 58.3 ppm for the C site at 127°, the hyperfine coupling constants of α-Tl(Se) were determined to be A_{Aa} = 15.2 kOe/μ_B and A_{Ab} = 19.4 kOe/μ_B at θ = 54°, A_B = 18.4 kOe/μ_B and A_C = 17.7 kOe/μ_B at θ = 127° Because the atomic parameters of α-Rb have not been determined, the chemical shift for α-Rb was previously calculated using the atomic parameters of α-NH_4 [22]. For systematic comparisons, however, the corresponding atomic parameters should be used. Hence XRD measurements for α-Rb and α-NH_4 were taken and the chemical shifts of α-Rb and α-NH_4 were evaluated using the following atomic parameters: For α-Rb, 59.4 ppm for the A site at 54°, 60.3 ppm for the B site at 127° and 58.6 ppm for the C site at 127°. for α-NH_4, 59.9 ppm for the A site at 56°, 62.6 ppm for the B site at 142° and 68.0 ppm for the C site at 142°. For α-Rb, the hyperfine coupling constants were determined to be A_{Aa} = 13.1 kOe/μ_B and A_{Ab} = 14.8 kOe/μ_B at θ = 54°, A_B = 14.7 kOe/μ_B and A_C = 14.0 kOe/μ_B at θ = 127°, whereas for α-NH_4, these constants were determined to be A_{Aa} = 12.8 kOe/μ_B and A_{Ab} = 14.2 kOe/μ_B at θ = 56°, A_B =13.7 kOe/μ_B and A_C = 11.7 kOe/μ_B at θ = 142°.

	θ	^{13}C site	δ (ppm)	σ (ppm)	K (ppm)	χ(250 K) (× 10^{-5} emu/mol)	A (kOe/μB)
α-NH_4	56°	A_a	441.5 [23]	59.9	381.6	16.6	12.8
	56°	A_b	554.0 [23]	59.9	494.1	19.4	14.2
	142°	B	368.1 [23]	62.6	305.5	12.5	13.7
	142°	C	283.0 [23]	68.0	215.0	10.3	11.7
α-Rb	54°	A_a	426.5 [22]	59.4	367.1	15.6	13.1
	54°	A_b	540.2 [22]	59.4	480.8	18.1	14.8
	127°	B	369.2 [22]	60.3	309.0	11.8	14.7
	127°	C	305.8 [22]	58.6	247.3	9.83	14.0
α-Tl(Se)	54°	A_a	426.7	59.8	366.9	12.6	15.2
	56°	A_b	526.9	59.8	467.1	14.3	19.4
	127°	B	350.9	60.2	290.7	8.83	18.4
	127°	C	256.3	58.3	198.0	6.25	17.7

Table 6.1: NMR parameters of α-(BEDT-TTF)$_2M$Hg(XCN)$_4$.

6.2 Temperature dependence of local spin susceptibilities

The temperature dependence of the NMR spectrum of α-Tl(Se) was determined at θ = 54° and 127° (Fig. 6.3). This spectrum enabled a determination of the temperature dependence of NMR shift for each peak (Fig. 6.4).

The NMR shifts of A_a, A_b, B, and C show different temperature dependence. Because the NMR shifts mainly reflect the local density of state [36], this behavior suggests that the B and C molecules could become the charge rich and poor sites due to the off-site Coulomb repulsion, respectively. Based on the estimated hyperfine coupling constants, the local spin susceptibilities could be determined. We also evaluated the local spin susceptibilities of α-Rb and α-NH_4 using reported temperature dependence of NMR shifts [22, 23] and the hyperfine coupling constants described in Sec.6.1.

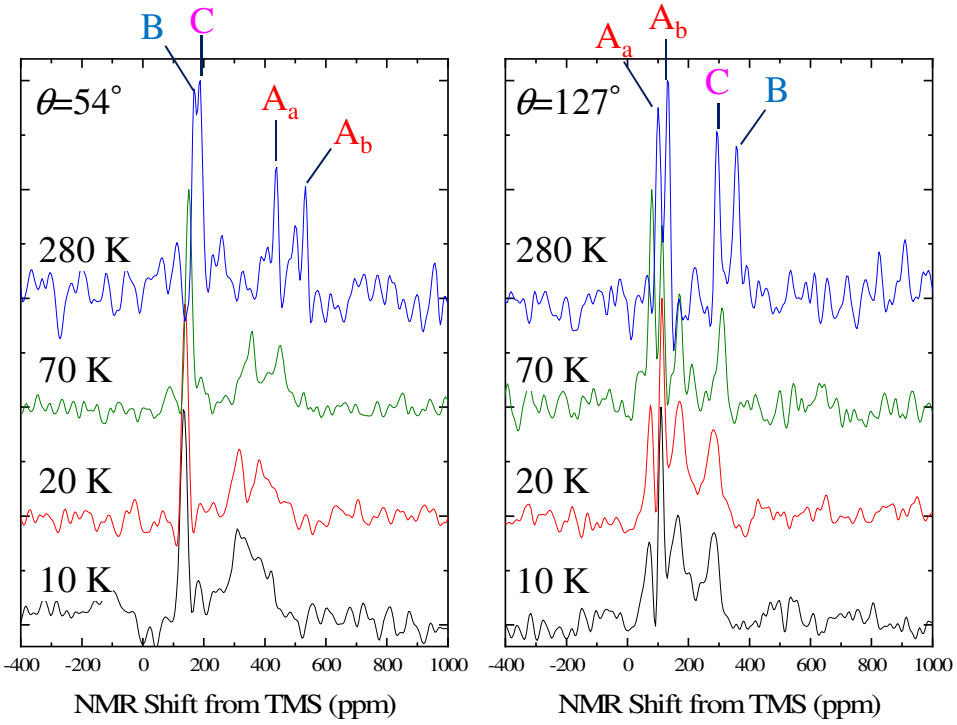

Figure 6.3: NMR spectrum of α-Tl(Se) with θ =54° and 127° at several temperatures.

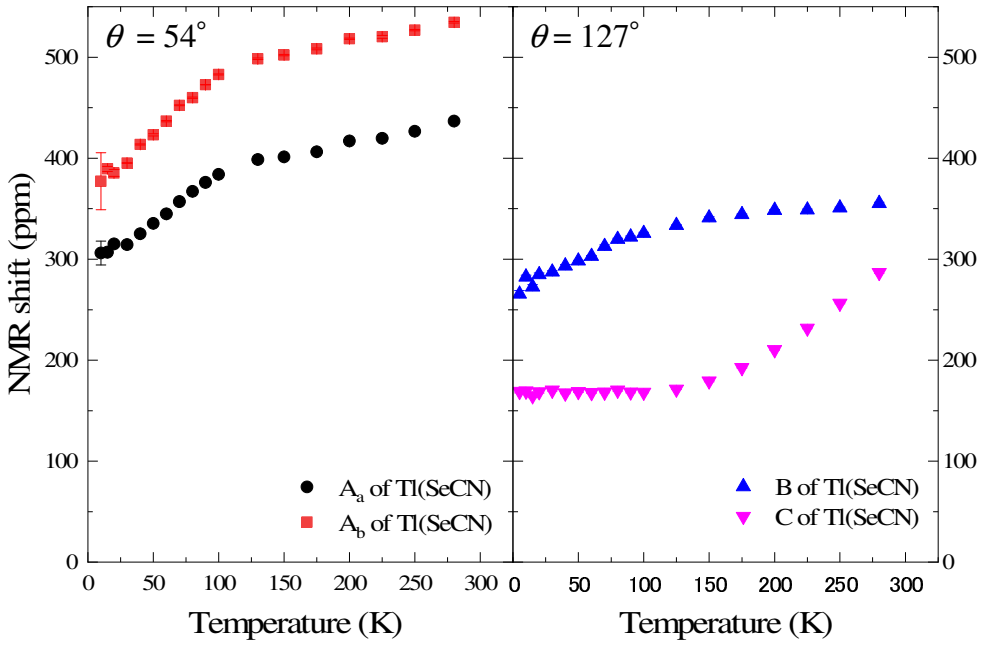

Figure 6.4: Temperature dependence of the NMR shift of α-Tl(Se). The NMR shift of the A_a and A_b sites were measured at θ =54° and those of the B and C sites at θ = 127°. The error bars indicate the uncertainty of the fits.

Figure 6.5(a) shows the temperature dependence of total spin susceptibilities ($\chi_{All} = 2\chi_A + \chi_B + \chi_C$), and Figures. 6.5(b)-(d) shows the ratios of local spin susceptibilities (χ_i/χ_{All}; i = A, B, and C) of α-Tl(Se), compared with those of α-NH_4 and α-Rb. Here, χ_A is the average spin susceptibilities of the A_a and A_b sites, with χ_A estimated from the NMR shift of the A site at θ = 54°, and χ_B and χ_C estimated from the NMR shifts of the B and C sites at θ = 127°. The total spin susceptibilities of α-Tl(Se) measured with a SQUID magnetometer (χ_{SQUID}) were denoted by black stars in Fig. 6.5 (a). The χ_{All} of α-Tl(Se) was consistent with its χ_{SQUID}.

The χ_A/χ_{All} showed almost the same temperature dependence, whereas χ_{All} showed different temperature dependences. At low temperatures, χ_B/χ_{All} ratios of α-NH_4, α-Rb, and α-Tl(Se) differed significantly, with the χ_B/χ_{All} ratio of α-Tl(Se) being the smallest. The χ_C/χ_{All} ratio showed the opposite behavior at the B site, with the χ_C/χ_{All} ratio of α-Tl(Se) being the largest.

Previous ^{13}C-NMR studies suggested that the χ_B/χ_A ratio at low temperature could tune the ground state of α-type salts [23]. The χ_B/χ_A of α-Tl(Se) was 0.7, much smaller than those of α-Rb and α-NH_4, which were 0.9.

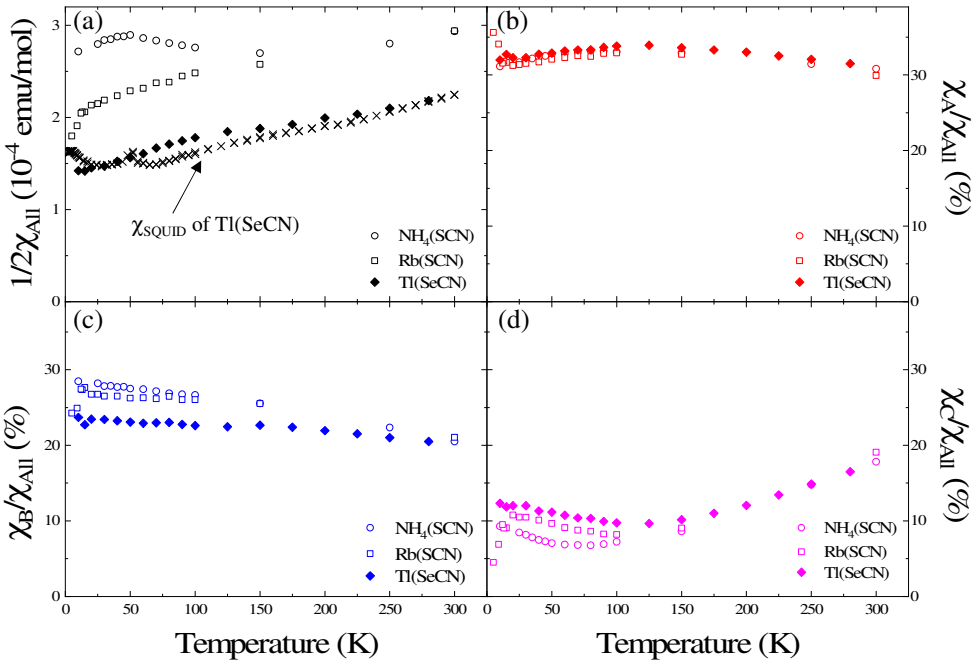

Figure 6.5: Temperature dependence of (a) total spin susceptibilities ($\chi_{\rm All} = 2\chi_{\rm A} + \chi_{\rm B} + \chi_{\rm C}$) and (b)-(d) ratios of local spin susceptibilities ($\chi_{\rm i}/\chi_{\rm All}$; i = A, B, and C). The black stars denote the spin susceptibility of α-Tl(Se) evaluated by SQUID measurements ($\chi_{\rm SQUID}$). The temperature dependence of NMR shifts of α-NH_4 and α-Rb salts were taken from the literatures [23, 22].

6.3 Temperature dependence of the NMR line width

Figure 6.6 shows the temperature dependence of the line widths of the NMR shift of the A, B, and C sites in α-Tl(Se) normalized relative to those at 300 K. The normalized line widths were 1.0±0.1 in the range from room temperature to 200 K, and showed similar behaviors. The line widths gradually increased below 100 K, however, this increase would not be related with T^* anomalies and would be attributed to the lattice degree of freedom rather than the charge disproportion because there is no site and sample dependence. The inset shows the temperature dependence of the line widths of the A sites in α-NH_4, α-Rb, and α-Tl(Se). In α-NH_4 and α-Rb, these line widths showed an anomaly at 230 K, with the line width of the A site gradually increasing below $T^* \simeq$ 200 K.

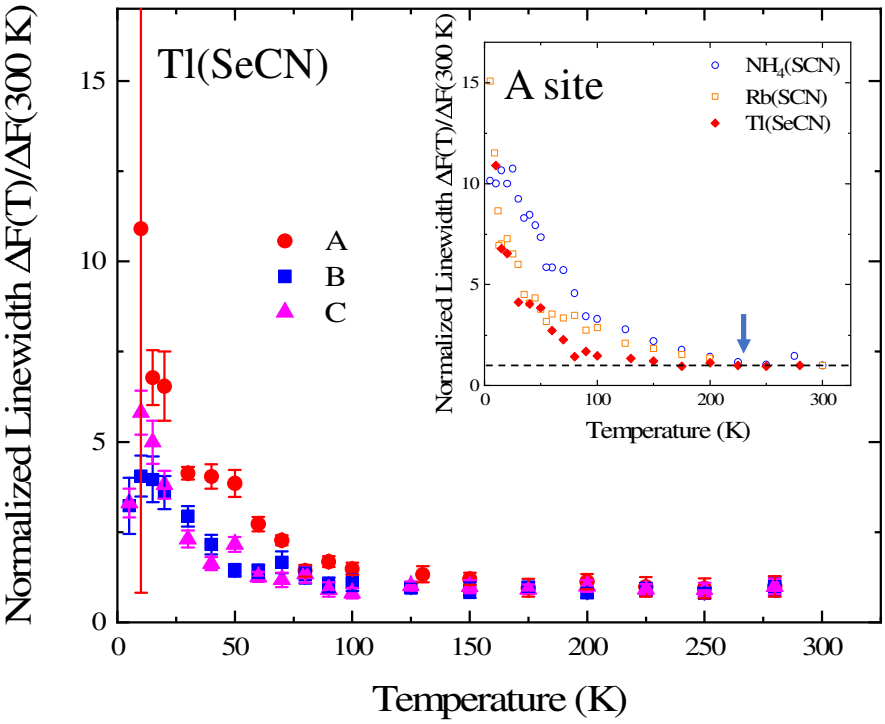

Figure 6.6: Temperature dependence of the line width of the NMR shifts of the A, B, and C sites in α-Tl(Se) normalized relative to those at 300 K. The error bars indicate the uncertainty of the fits. The inset shows the temperature dependence of the line widths of the A sites in α-NH_4, α-Rb [23, 22], and α-Tl(Se).

In contrast, the line widths of the B and C sites did not show anomalies at $T^* \simeq 200$ K. Because A molecules are located in a general position and are connected by inversion symmetry, the line broadening of A molecules may be attributed to the instability due to the breakage of inversion symmetry at 200 K, a finding also observed by infrared vibrational spectroscopy [24]. In α-Tl(Se), however, the line width of the A site did not increase below $T^* \simeq 200$ K and remained as sharp as the line widths of the B and C sites, suggesting that the instability was suppressed and there is no anomaly in α-Tl(Se). From the inset of Fig. 6.6, the anomaly of α-NH_4 and α-Rb is expected to develop at 230 K.

6.4 The anomaly at T^*

The behavior of α-Tl(Se) was consistent with the absence of the anomaly at $T^* \simeq 230$ K, a line broadening observed in α-Rb and α-NH_4. Optical

studies reported additional absorption by the CDW salt of α-K and the linear thermal expansion coefficient of α-NH_4 shows a weak maximum, which could represent a pseudogap in charge fluctuation [20, 37]. However, because line broadening of the A site was not so large [22, 23] and whether the disproportionation in A column develops or not was unclear, the relationships among T^* anomalies, pseudogaps and charge disproportionation was unclear.

Figure 6.8 shows the temperature dependence of χ_B/χ_C in α-Tl(Se), α-NH_4 and α-Rb. At room temperature, χ_B and χ_C were almost identical in all α-type salts, suggesting no charge disproportionation in the BC column of Fig. 6.1. Because the A sites are crystallographically equivalent and because charge disproportionation is not observed in the A column at room temperature, no α-type salt shows significant charge disproportionation at room temperature.

The χ_B/χ_C ratio gradually increased with decreasing temperature. Because χ_A/χ_{All} is almost temperature independent in all α-type salts (see Sec. 6.2, above), no α-type salt showed evidence of vertical stripe disproportionation, with the increase in χ_B/χ_C indicating a develop of inhomogeneity between B and C molecules. However, the B and C molecules are crystallographically independent, such that their develop of inhomogeneity did not require a disruption of symmetry. Hence the association between anomalies at $T^* \simeq 230$ K and increases in χ_B/χ_C were unclear.

Although the χ_B/χ_C ratios of α-Rb and α-NH_4 continued to increase with decreasing temperature, the χ_B/χ_C ratio of α-Tl(Se) deviated below $T^* \simeq 230$ K and decreased at low temperatures. As the temperature of 230 K is consistent with the temperature of line width anomaly at A site, the temperature dependence of χ_B/χ_C suggests an association between T^* anomalies and the develop of inhomogeneity between B and C molecules in both CDW and SC salts. The greater inhomogeneity between B and C molecules observed in α-Rb and α-NH_4 at low temperatures suggests that the line broadening in A sites corresponds to the instability of the horizontal stripe modulation. Note that the horizontal stripe modulation might not be the static modulation but the fluctuated modulation. The line broadening in A sites is not so drastic, suggesting that the inversion symmetry between A molecules would not completely be broken and this modulation would be fluctuated as shown in Fig. 6.7. The degree of the fluctuation would increase with decreasing temperature without a phase transition.

CDW and SC salts showed the development of horizontal stripe modulation below $T^* \simeq 230$ K, suggesting that the T^* anomalies, pseudogaps and line broadening in the A column, were due to horizontal stripe modulation. The instability due to horizontal stripe modulation may contribute to superconductivity.

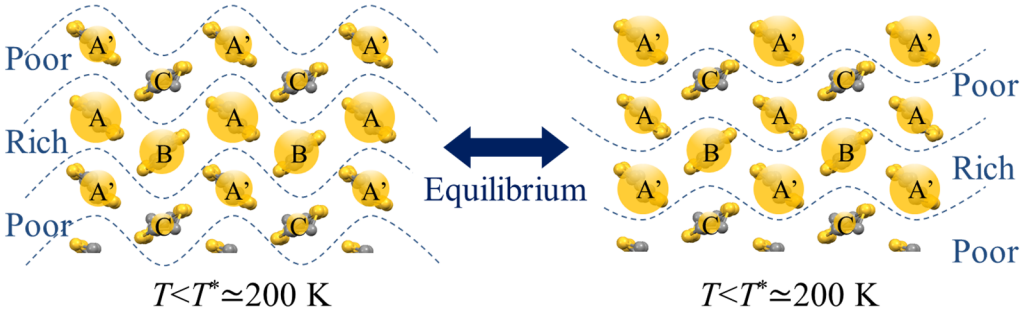

Figure 6.7: The schematic diagram of the horizontal stripe modulation below T^*. While B and C molecules are crystallographically independent and become rich and poor sites, respectively, A molecules are connected by the inversion symmetry and are fluctuated.

From previous NMR study, the χ_B/χ_A phase diagram was proposed, where the SC and metallic salts were located in large and small χ_B/χ_A regions, respectively [23]. The χ_B/χ_A would mainly reflect the degree of the horizontal stripe modulation, χ_B/χ_C or χ_B/χ_{All} because the χ_A/χ_{All} showed almost the same temperature dependence in all α-type salts (Fig. 6.5(b)).

The degree of the modulation, χ_B/χ_C, may be inherited from the crystal structure. As mentioned in Sec. 3.6, the SC salt may be located in the small V_{A-B}/t_B and large V_{A-C}/t_C region from Fig. 3.10, suggesting that the electron may move more easily from charge rich A molecule to charge poor B molecule while that move more difficultly from A molecule to charge poor C molecule in SC salt than in metallic salt. As a result, the degree of the modulation may be enhanced in the SC salt while that may be suppressed in the metallic salt. Systematic analyses of the temperature dependence of the crystal structures or crystal parameters in α-type salts are desired.

The χ_B/χ_C of α-NH_4 deviated from that of α-Rb below 120 K and had a broad maximum around 50 K. This difference is that may have been due to the effects of NH_4^+ rotation on electronic properties. ^{2}D-NMR measurements suggested a change in motion of NH_4^+ at 130 K and an order-disorder like transition in the anion layer at 25-40 K [16]. However, the spin susceptibility of α-NH_4(Se) indicated that the motion of NH_4^+ had no effect on its electronic properties [35] as mentioned in Sec. 3.3. A detailed study of NH_4^+ in α-NH_4 and α-NH_4(Se) is required to reveal its effect on electronic properties.

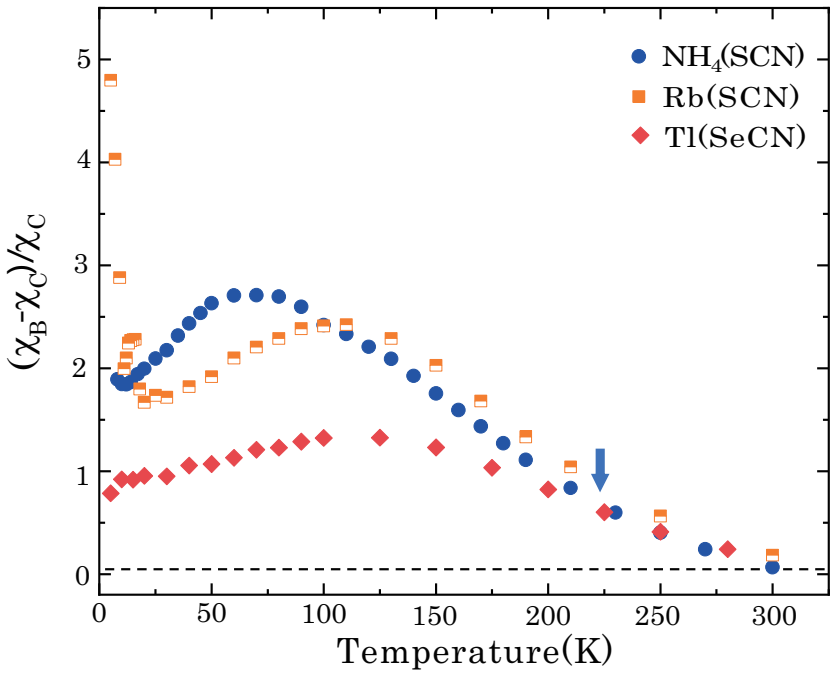

Figure 6.8: Temperature dependence of χ_B/χ_C in α-Tl(Se), α-NH_4, and α-Rb.

6.4.1 Horizontal stripe modulation in α-(BEDT-TTF)$_2M$Hg(XCN)$_4$ and α-(BEDT-TTF)$_2$I$_3$ salts

The inhomogeneity between B and C molecules and the line-broadening between A molecules in the CDW and SC salts below $T^*\simeq$ 230 K resulted from the instability of horizontal stripe modulation. Similarly, horizontal stripe modulation in metallic state was reported in α-(BEDT-TTF)$_2$I$_3$ [abbreviated I$_3$] [25]. Similar to α-(BEDT-TTF)$_2M$Hg(XCN)$_4$ salts, three crystallographic A, B, and C molecules were present in I$_3$. We defined the B and C molecules of α-(BEDT-TTF)$_2$I$_3$ as C and B molecules of α-(BEDT-TTF)$_2M$Hg(XCN)$_4$, respectively, because these molecules become poor and rich sites, respectively. Site selective ^{13}C-NMR of I$_3$ revealed that the inhomogeneity between B and C molecules in I$_3$ increased with decreasing temperature [38, 39]. Below 135 K, the I$_3$ became an insulator, with the horizontal stripe charge ordering (CO) state, confirmed by optical, NMR, and XRD analyses [40, 41, 42].

The degree of charge disproportionation was assessed by plotting the χ_B/χ_C ratio of the paramagnetic state of I$_3$ against that of α-(BEDT-TTF)$_2M$Hg(XCN)$_4$ salts (Fig. 6.9). Despite differences in their Fermi surfaces, the χ_B/χ_C ratio of the I$_3$ in the paramagnetic state slightly increased

with decreasing temperature and no anomaly in NMR linewidth of the A sites was observed above 135 K, as in α-(BEDT-TTF)$_2M$Hg(XCN)$_4$ salts. Because off-site Coulomb repulsion is sensitive to molecular arrangement, this result suggests that the instability due to a horizontal stripe modulation could be a common feature of α-type salts.

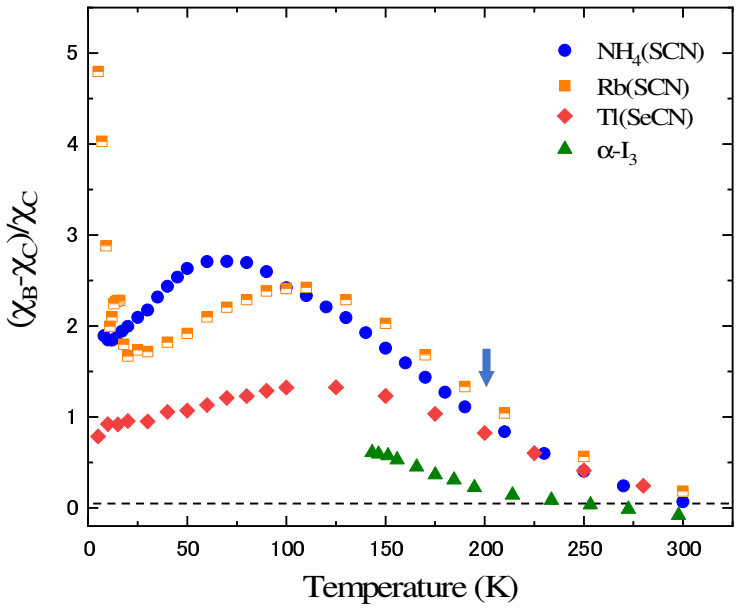

Figure 6.9: Temperature dependence of χ_B/χ_C in α-Tl(Se), α-NH$_4$, α-Rb and α-(BEDT-TTF)$_2$I$_3$.

Chapter 7

Summary

The electronic structures of the metallic salt of α-Tl(Se) were compared with those of α-Rb and α-NH_4 by ^{13}C-NMR measurements, revealing relationships among T^* anomalies, pseudogaps and line broadening. Although $\chi_{\rm All}$ showed different temperature dependences among the CDW, SC, and metallic salts, the $\chi_{\rm A}/\chi_{\rm All}$ showed almost the same temperature dependence, suggesting that no α-type salts showed evidence of vertical stripe disproportionation. The NMR line width of the A sites and the $\chi_{\rm B}/\chi_{\rm C}$ ratios in α-Rb and α-NH_4 increased, deviating from those in α-Tl(Se) below $T^*\simeq$ 230 K. These results suggest the instability of the horizontal stripe modulation develops below 230 K and the pseudogap observed in an optical study is due to the formation of the horizontal stripe modulation. The degree of the horizontal stripe modulation would be consistent with the proposed $\chi_{\rm B}/\chi_{\rm A}$ phase diagram. Below T^*, the instability of the horizontal stripe modulation could contribute to superconductivity. Because the horizontal stripe CO state was suggested to occur in I_3 below 135 K, the $\chi_{\rm B}/\chi_{\rm C}$ ratios of the paramagnetic state of I_3 and α-(BEDT-TTF)$_2M$Hg(XCN)$_4$ salt were compared. Despite differences in their Fermi surfaces, the $\chi_{\rm B}/\chi_{\rm C}$ of I_3 increased with decreasing temperature, as in α-(BEDT-TTF)$_2M$Hg(XCN)$_4$ sats, suggesting that instability due to horizontal stripe modulation could be a common feature of α-type salts.

Chapter 8

Acknowledgement

I would like to express my gratitude to Professor Atushi Kawamoto, Yoshihiko Ihara, and Shuhei Fukuoka for their guidances and many advices. I would like to acknowledge Professor Kazushige Nomura, Professor Migaku Oda , and Professor Koichi Hiraki in the review process of my doctoral thesis. I would like to thank K. Noda and T. Kawai for helpful discussions and experimental data of the α-Rb and α-NH_4. I would like to thank Dr Y. Fukuda and N. Akiko of Ochanomizu University for determination of the crystal structure. I would like to thank Professor Yukihiro Takahashi of Hokkaido University for determination fo the crystal structure of the α-NH_4(Se) and so on. I would like to thank Professor Hiromi Taniguchi of Saitama University for resistivity measurement of α-NH_4(Se). I would like to thank members of Low Temperature Physics Group in Hokkaido University for their kind assistance.

I am grateful for the financial support given by Ushio Foundation, Kawamura Scholaship Foundation and Advanced Program of Nitobe School. These studies were supported by KAKENHI Grant No. 16K05427 and Hokkaido University Global Facility Center (GFC), Advanced Physical Property Open Unit(APPOU), funded by MEXT under the Support Program for Implementation of New Equipment Sharing system.

Finally, I would like to thank my family for their supports and encouragement.

Bibliography

[1] R. Shibaeva and L. Rozenberg, Crystallography Reports **39**, 47 (1994).

[2] H. Mori *et al.*, Solid State Communications **74**, 1261 (1990).

[3] T. Sasaki *et al.*, Journal of the Physical Society of Japan **65**, 213 (1996).

[4] R. Shibaeva, L. Rozenberg, N. Kushch and E. Yagubskii, Crystallography Reports **39**, 747 (1994).

[5] H. Mori *et al.*, Bulletin of the Chemical Society of Japan **63**, 2183 (1990).

[6] N. Kushch *et al.*, Synthetic Metals **46**, 271 (1992).

[7] T. Sasaki and N. Toyota, Solid State Communications **75**, 93 (1990).

[8] N. Kihoshita, M. Tokumoto and H. Anzai, Journal of the Physical Society of Japan **60**, 2131 (1991).

[9] H. Wang *et al.*, Physica C: Superconductivity **166**, 57 (1990).

[10] T. Sasaki and N. Toyota, Physical Review B **49**, 10120 (1994).

[11] M. V. Kartsovnik, A. E. Kovalev and N. D. Kushch, Journal de Physique I **3**, 1187 (1993).

[12] S. Uji *et al.*, Physical Review B **54**, 9332 (1996).

[13] L. I. Buravov *et al.*, Journal de Physique I France **4**, 441 (1994).

[14] K. Miyagawa, A. Kawamoto and K. Kanoda, Synthetic Metals **86**, 1987 (1997).

[15] T. Sasaki, S. Endo and N. Toyota, Physical Review B **48**, 1928 (1993).

[16] S. Endo *et al.*, Physical Review B **57**, 14422 (1998).

[17] M. Maesato, Y. Kaga, R. Kondo and S. Kagoshima, Physical Review B **64**, 155104 (2001).

[18] P. Foury-Leylekian, S. Ravy, J.-P. Pouget and H. Müller, Synthetic Metals **137**, 1271 (2003).

[19] N. Drichko *et al.*, Physical Review B - Condensed Matter and Materials Physics **74**, 235121 (2006).

[20] M. Dressel, N. Drichko, J. Schlueter and J. Merino, Physical review letters **90**, 167002 (2003).

[21] J. Merino and R. H. McKenzie, Physical Review Letters **87**, 2370021 (2001).

[22] K. Noda, Y. Ihara and A. Kawamoto, Physical Review B **87**, 085105 (2013).

[23] Y. Ihara and A. Kawamoto, Physical Review B **90**, 041107 (2014).

[24] T. Hiejima, S. Yamada, M. Uruichi and K. Yakushi, Physica B: Condensed Matter **405**, S153 (2010).

[25] K. Bender *et al.*, Molecular Crystals and Liquid Crystals **108**, 359 (2007).

[26] M. Watanabe, Y. Noda, Y. Nogami and H. Mori, Journal of the Physical Society of Japan **73**, 116 (2004).

[27] G. M. Sheldrick, Acta Crystallographica **64**, 112 (2008).

[28] T. Mori, H. Mori and S. Tanaka, Bulletin of the Chemical Society of Japan **72**, 179 (1999).

[29] K. Miyagawa, A. Kawamoto and K. Kanoda, Physical Review B **56**, R8487 (1997).

[30] H. Mori, S. Tanaka and T. Mori, Physical Review B **57**, 12023 (1998).

[31] G. E. Pake, The jounal of Chemical Physics **16**, 327 (1948).

[32] K. Kanoda, Hyperfine Interactions **104**, 235 (1997).

[33] T. Klutz, I. Hennig, U. Haeberlen and D. Schweitzer, Applied Magnetic Resonance **2**, 441 (1991).

[34] Y. Takano, K. Hiraki, Y. Takada, H. M. Yamamoto and T. Takahashi, Journal of the Physical Society of Japan **79**, 104704 (2010).

[35] A. Ohnuma, H. Taniguchi, Y. Takahashi and A. Kawamoto, The Journal of Physical Chemistry C **122**, 24321 (2018).

[36] K. Miyagawa, A. Kawamoto and K. Kanoda, Physical Review B **62**, 7679 (2000).

[37] A. Dolbin, M. Khlistyuck, N. A. Vinnikov and R. Basnukaeva, Low Temperature Physics **45**, 128 (2019).

[38] T. Kawai and A. Kawamoto, Journal of the Physical Society of Japan **78**, 074711 (2009).

[39] S. Hirose and A. Kawamoto, Physical Review B **82**, 115114 (2010).

[40] R. Wojciechowski, K. Yamamoto, K. Yakushi, M. Inokuchi and A. Kawamoto, Physical Review B - Condensed Matter and Materials Physics **67**, 224105 (2003).

[41] S. Moroto *et al.*, Journal de Physique IV (Proceedings) **114**, 399 (2004).

[42] T. Kakiuchi, Y. Wakabayashi, H. Sawa, T. Takahashi and T. Nakamura, Journal of the Physical Society of Japan **76**, 113702 (2007).